Constitutively active RAS in *S. pombe* causes persistent Cdc42 signalling but only transient MAPK activation

Emma J. Kelsall[1,8], Ábel Vértesy[2,6,8], Kees Straatman[3], Mishal Tariq[1], Raquel Gadea[1,4], Chandni Parmar[1], Gabriele Schreiber[2], Shubhchintan Randhawa[1,7], Cyril Dominguez[1,5], Edda Klipp[2]* and Kayoko Tanaka[1,9]*

1 Department of Molecular and Cell Biology, University of Leicester

2 Theoretical Biophysics, Institute of Biology, Humboldt-Universität zu Berlin

3 Centre for Core Biotechnology Services, University of Leicester

4 Marco Formacion Profesional, Calle del Conde de Aranda 7-9, 50004 Zaragoza, Spain

5 Leicester Institute of Structural and Chemical Biology, University of Leicester

6 Present address: Hubrecht Institute-KNAW (Royal Netherlands Academy of Arts and Sciences) and University Medical Center, 3584 CT Utrecht, The Netherlands

7 Present address: Sanjay Gandhi Post Graduate Institute of Medical Sciences, Department of Molecular Medicine & Biotechnology, Lucknow, India 226014

8 These authors contributed equally

9 Lead Contact

*Correspondence: kt96@le.ac.uk (K.T.), edda.klipp@rz.hu-berlin.de (E.K.)

Highlights

(1) Constitutive Ras1.GV causes over-activation of Cdc42 in *S. pombe* pheromone signaling

(2) Ras1.GV induces an acute but only transient MAPK^{Spk1} activation

(3) The RAS effector pathways MAPK^{Spk1} and Cdc42 compete with each other for active Ras1

(4) Predictive modelling explains MAPK^{Spk1} activation dynamics in 24 signaling-mutants

eTOC Blurb

S. pombe Ras1 activates the MAPK^{Spk1} and Cdc42 pathways. Kelsall et al. report that the constitutively active Ras1.G17V mutation, which causes morphological anomalies, induces prolonged Cdc42 activation and MAPK^{Spk1} activation followed by attenuation. Mathematical modelling shows competition between the MAPK^{Spk1} and Cdc42 pathways for active Ras1.

Summary

The small GTPase RAS is a signalling hub. Oncogenic RAS mutations are assumed to over-activate all of the downstream pathways. We tested this assumption in fission yeast, where, RAS-mediated pheromone signalling (PS) activates the MAPK^{Spk1} and Cdc42 pathways. Unexpectedly, we found that constitutively active Ras1.G17V induced acute transient MAPK^{Spk1} activation, whilst Cdc42 activation persisted. Acute transient MAPK^{Spk1} activation was also seen in the deletion mutant of Cdc42-GEF^{Scd1}, a Cdc42 activator. We have built a mathematical model using PS negative-feedback circuits and competition between the two Ras1 effectors, MAPKKK^{Byr2} and Cdc42-GEF^{Scd1}. The model robustly predicted the MAPK^{Spk1} activation dynamics of an additional 21 PS mutants. Supporting the model, we show that a recombinant Cdc42-GEF^{Scd1} fragment competes with MAPKKK^{Byr2} for Ras1 binding. Our study has established a concept that constitutive RAS yields biased Cdc42/Rac over-activation, providing a strong rationale to interfere with this process to target oncogenic RAS in humans.

Key words

Ras, MAPK, Cdc42/Rac, yeast pheromone signalling

Introduction

Proto-oncogene Ras GTPase family members are widely conserved and play pivotal roles in cell growth, differentiation and apoptosis (Cox and Der, 2010). The physiological impact of Ras mutations is highlighted in the resultant tumorigenesis and developmental disorders (Prior et al., 2012; Schubbert et al., 2007). More than 99% of identified oncogenic RAS mutations occur at codons 12, 13 and 61 of human Ras isoforms (Prior et al., 2012) and impair efficient GTP hydrolysis (Trahey and McCormick, 1987). This results in accumulation of GTP-bound Ras, which is generally considered to cause constitutive activation of the downstream effector pathways, such as ERK and PI3K signalling pathways (Lin et al., 1998; Zhu et al., 1998). Interestingly, mouse embryonic fibroblasts (MEFs) derived from the *K-ras*^{G12D} mouse model show neither an increased basal level of active ERK and Akt nor constitutive activation of ERK and Akt upon growth factor stimulation even though the *K-ras*^{G12D} MEFs showed enhanced proliferation and partial transformation (Tuveson et al., 2004). This observation indicates that not all effector pathways become constitutively activated by oncogenic Ras, presumably because of an efficient negative feedback loop. Meanwhile, it is reasonable to expect that oncogenic RAS over-activates some of its effector pathways to initiate tumorigenesis. Small GTPases, including Cdc42 and Rac, may be such effector pathways, as they are required in oncogenic-RAS-driven tumorigenesis (Malliri et al., 2002; Qiu et al., 1997; Stengel and Zheng, 2012).

We wished to understand how multiple Ras effector pathways respond to the Ras-triggered signals in a physiological setting. We employed the model organism fission yeast. In this organism, a unique Ras homologue, Ras1, plays a key role in pheromone signalling to cause mating of haploid cells and sporulation in diploid cells (Yamamoto, 1996)(Fig. 1A, B). Upon nutritional starvation, cells of opposite mating types (h^+ and h^-) exchange mating pheromones. Gpa1, the α-subunit of the pheromone receptor-coupled G-protein, relays the pheromone signal into the cell (Obara et al., 1991). Activated Gpa1 together with Ras1 then activate MAPK cascade consisting of Byr2 (MAPKKK), Byr1 (MAPKK) and Spk1 (MAPK) (Fukui et al., 1986; Masuda et al., 1995; Nadin-Davis and Nasim, 1988; Nadin-Davis et al., 1986a; Nadin-Davis et al., 1986b; Wang et al., 1991; Xu et al., 1994). An intriguing observation is that the *ras1.G17V* mutant, an equivalent of mammalian *ras.G12V* mutant prevalent in cancer, produces an excessively elongated shmoo, or a conjugation tube, upon exposure to the mating pheromone (Nadin-Davis et al., 1986a). This “elongated” *ras1.G17V* phenotype has been interpretted that

Ras1 might be directly responsible for amplifying the pheromone signal at an intracellular level (Yamamoto, 1996).

Ras1 also regulates cell morphology during vegetative growth; whilst deletion of either *gpa1*, *MAPKKK*^{byr2}, *MAPKK*^{byr1} or *MAPK*^{spk1} does not result in any obvious phenotypes during vegetative cell growth (Obara et al., 1991; Sipiczki, 1988; Toda et al., 1991), *ras1⊿* cells lose the typical rod-shape morphology of fission yeast to become rounded (Fukui et al., 1989; Nadin-Davis et al., 1986a). Studies based on recombinant protein assays and yeast-2-hybrid analysis demonstrated that Ras1 interacts with both MAPKKK^{Byr2} and Scd1, a GDP-GTP exchange factor (GEF) for Cdc42, which regulates the actin cytoskeleton and cell morphology (Chang et al., 1994; Gronwald et al., 2001; Tu et al., 1997). These observations suggest that Ras1 simultaneously regulates both the pheromone MAPK^{Spk1} and the Cdc42 pathways at the cell membrane (Weston et al., 2013). Indeed, a dynamic "Cdc42 zone" at the cell cortex prior to mating has been observed (Merlini et al., 2013) and Ras1 and MAPK^{Spk1} cascade components are found there and are involved in the process (Dudin et al., 2016; Merlini et al., 2013; Merlini et al., 2016; Merlini et al., 2018; Weston et al., 2013). However, it is not yet understood how Ras1 interplay between the two pathways. By establishing conditions to induce highly synchronous mating of fission yeast cells, for the first time we were able to follow MAPK^{Spk1} activation during the physiological mating process in wildtype and in mutants showing various mating phenotypes. This comprehensive set of quantitative measurements allowed us to build a mathematical model of the Ras-mediated pheromone signalling. Our model can serve as a prototype of a branched Ras-mediated signalling pathway, demonstrating a competition of downstream pathways for a common upstream activator, Ras1. The model also highlights the physiological importance of the bipartite activation of MAPKKK^{Byr2}: a Ras1-dependent and a Ras1-independent mechanism, the latter of which employs the adaptor protein Ste4 (Barr et al., 1996; Okazaki et al., 1991). The adaptor^{Ste4} can be targeted to downregulate MAPK^{Spk1} even in the presence of *ras1.G17V* mutation. Finally, our study reveals the crucial role played by Cdc42 in the *ras1.G17V* mutant causing the *ras1.G17V* phenotype.

Results

(1) A highly synchronous mating assay allows the precise measurement of MAPK^{Spk1} activity

To directly measure fission yeast pheromone signalling, we quantitated MAPK^{Spk1} phosphorylation throughout the mating process (Fig. S1, Fig. 1A and B). We established a protocol to induce highly synchronous mating and employed cells where the endogenous MAPK^{Spk1} is tagged with GFP-2xFLAG. Under these conditions, homothallic *h^{90}* cells started to mate 7-hours after induction of mating (Fig. 1C, grey line). Phosphorylated (active) MAPK^{Spk1} (**pp**MAPK^{Spk1}) levels were quantitated as described in Materials and Methods.

The **pp**MAPK^{Spk1} signal was first detected three hours after induction of mating and reached its peak at about seven hours, when cell fusion was also initially observed (Fig. 1C, blue line). The **pp**MAPK^{Spk1} then gradually decreased to a non-zero level as meiosis continued towards sporulation. The observation established that the MAPK^{Spk1}-GFP activation occurs as the mating process progresses and declines before sporulation, around 15 hours post induction. It was also noted that the total MAPK^{Spk1}-GFP was essentially not expressed during the vegetative cycle, but it was promptly induced by nitrogen starvation (Supplementary Fig. S2A and S2B). The *mapk^{spk1}* gene is a known target of the transcription factor Ste11 (Mata and Bahler, 2006), which itself is activated (phosphorylated) by MAPK^{Spk1} (Kjaerulff et al., 2005). This positive feedback loop likely facilitates a swift increase of MAPK^{Spk1} expression upon nitrogen starvation. We found that MAPK^{Spk1}-GFP localised to both the cytosol and the nucleus, with some nuclear accumulation, before it gradually disappeared as the mating process came to the end (Fig. 1D). Interestingly, transient foci of GFP signals were also found at the cell cortex, as has been reported for MAPKK^{Byr1}, the activator of MAPK^{Spk1} (Dudin et al., 2016) (Fig. 1D, yellow arrows).

(2) Constitutively active MAPKK$^{Byr1.DD}$ mutant causes constitutive activation of MAPK^{Spk1}

Activation of MAPKK family kinases is mediated by dual phosphorylation of conserved Ser/Thr residues (Zheng and Guan, 1994). These correspond to serine 214 and threonine 218 of the MAPKK^{Byr1}. A MAPKK^{Byr1} mutant termed MAPKK$^{Byr1.DD}$, which carries aspartic acid substitution at these sites, was expected to act as a constitutively active MAPKK (Ozoe et al., 2002). We introduced the *MAPKK$^{byr1.DD}$* mutation at its chromosome locus and measured the activation profile of its target, MAPK^{Spk1} during the mating process. The increase of the **pp**MAPK^{Spk1} signal in the *MAPKK$^{byr1.DD}$* mutant strain was delayed compared to the wildtype strain and the

143 **pp**MAPK^{Spk1} accumulated at a slower rate (Fig. 1E, light green line). However, the level of
144 **pp**MAPK^{Spk1} remained high after reaching its highest intensity at around 16 hours after
145 induction, resulting in a constitutive phosphorylation of MAPK^{Spk1} (Fig. 1E and Supplementary
146 Fig. S2C and S2D). This result highlights that the suggested de-phosphorylation of **pp**MAPK^{Spk1}
147 by phosphatases Pmp1 and Pyp1 (Didmon et al., 2002) is not efficient in downregulating the
148 pheromone signalling in the presence of MAPKK$^{Byr1.DD}$. The MAPKK$^{Byr1.DD}$ strain is also less
149 competent in finding the partner mating cell than cells with wildtype MAPKK^{Byr1}. We also
150 confirmed the intriguing "*fus*" (fusion deficient) phenotype of cells expressing MAPKK$^{Byr1.DD}$ from
151 its native promoter (Fig.1F) (Dudin et al., 2016; Ozoe et al., 2002). These cells find their partners
152 and pair up successfully but fail to fuse with each other, resulting in *fus* phenotype. Consistent
153 with the observed slower increase in **pp**MAPK^{Spk1} (Fig.1E) the nuclear localisation of MAPK^{Spk1}
154 was also delayed compared to Wildtype cells (Fig 1F). A strong MAPK^{Spk1}-GFP signal was then
155 observed in the nuclei of the paired *fus* cells and the nuclear MAPK^{Spk1}-GFP signal persists even
156 24 hours after the induction of mating (Fig. 1F). Interestingly, the projection tips of the paring
157 cells often show increased MAPK^{Spk1}-GFP signal (Fig. 1F, yellow arrows). These results conclude
158 that MAPK^{Spk1} activation is highly influenced by the MAPKK^{Byr1} status and phosphatases directly
159 regulating MAPK^{Spk1} cannot counteract MAPKK$^{Byr1.DD}$.
160
161 **(3) The *ras1.G17V* mutation causes acute transient MAPK^{Spk1} activation**
162 The fission yeast equivalent of human oncogenic *ras.G12V* is *ras1.G17V,* which induces an
163 excessively elongated shmoo, and the cells fail to recognize a partner and become sterile (Fukui
164 et al., 1986; Nadin-Davis et al., 1986a). The "elongated shmoo" phenotype was interpreted as
165 an excess activation of the downstream pathway(s) of Ras1, leading to a prediction that the
166 *ras1.G17V* causes over-activation of MAPK^{Spk1} (Weston et al., 2013; Yamamoto, 1996). However,
167 no direct evidence has been provided.
168 Quantitation of the **pp**MAPK^{Spk1}-GFP in the *ras1.G17V* mutant showed an acute increase of the
169 **pp**MAPK^{Spk1}-GFP upon induction of mating (Fig. 1G, Green line). However, the signal intensity
170 declined gradually and by 16 hours after induction the level was comparable to wildtype cells,
171 indicating that down-regulation of **pp**MAPK$^{Spk1\text{-}GFP}$ is effective, unlike in *MAPKK$^{byr1.DD}$* mutant.
172 Correspondingly, the cellular MAPK^{Spk1}-GFP signal also declined 24 hours after induction of
173 mating (Fig. 1H). Collectively, these observations indicate that the down-regulation mechanism
174 for **pp**MAPK^{Spk1} is robust and resistant to Ras1.G17V. It was also noted that the peak intensity of

the **pp**MAPK^{Spk1} was somewhat lower and the rate of signal reduction was slightly decreased compared to wildtype cells (Fig. 1G).

(4) The elongated *ras1.G17V* shmoos develop with a minimum level of MAPK^{Spk1}: neither amplitude nor duration of ppMAPK^{Spk1} signal influences the *ras1.G17V* phenotype

Having observed that *MAPKK$^{byr1.DD}$* and *ras1.G17V* show different MAPK^{Spk1} activation profiles (sustained vs transient) and different morphological phenotypes ("*fus*" vs elongated), we examined a link between the MAPK^{Spk1} activation profiles and the cell morphology. The MAPK^{Spk1} phosphorylation profile of the cells harbouring both *ras1.G17V* and *MAPKK$^{byr1.DD}$* mutations (*ras1.G17V MAPKK$^{byr1.DD}$* double mutant) was comparable to the cells harbouring *MAPKK$^{byr1.DD}$* mutation only; it showed a slow increase of the **pp**MAPK^{Spk1}-GFP level, which reached the plateau at about 16 hours after induction of mating (Fig. 2A, red line). The nuclear **pp**MAPK^{Spk1}-GFP signal in the *ras1.G17V MAPKK$^{byr1.DD}$* double mutant was also present 24 hours after induction of mating, unlike the *ras1.G17V* single mutant cells, confirming that the *ras1.G17V MAPKK$^{byr1.DD}$* double mutant cells retained a high **pp**MAPK^{Spk1} level. Thus, in terms of the activation status of MAPK^{Spk1}, *MAPKK$^{byr1.DD}$* is epistatic to *ras1.G17V*.

In terms of cell morphology, the *ras1.G17V MAPKK$^{byr1.DD}$* double mutant cells showed the "elongated" *ras1.G17V* phenotype (Fig. 2B), but not the "paired" *MAPKK$^{byr1.DD}$* phenotype. Therefore, *ras1.G17V* was epistatic to *MAPKK$^{byr1.DD}$* in terms of the elongated shmoo morphology.

Interestingly, obvious shmoo formation in the *ras1.G17V MAPKK$^{byr1.DD}$* double mutant was first noticed 16 hours after induction of mating, much later than the *ras1.G17V* single mutant, but as a similar timing as the *MAPKK$^{byr1.DD}$* single mutant (Fig. 2B). Given the slow increase of the **pp**MAPK^{Spk1} signal in mutants harbouring the *MAPKK$^{byr1.DD}$* mutation, we predicted that the delayed appearance of the *ras1.G17V* shmoo meant that the *ras1.G17V* shmoo formation still requires a certain level of MAPK^{Spk1} activity. Indeed, when *MAPKK^{byr1}* was deleted in the *ras1.G17V* mutant, not only was the MAPK^{Spk1} activation and nuclear MAPK^{Spk1}-GFP signal abolished (Fig. S1F), but also shmoo formation was abrogated as in the *MAPKK$^{byr1}\Delta$* single mutant (Fig. 2C). Based on these observations, we concluded that the cell morphology is determined by the molecular status of Ras1, and not by the MAPK^{Spk1} activation profile. Yet, the *ras1.G17V* phenotype still requires MAPK^{Spk1} activity, which determines the timing of shmoo formation.

(5) Cdc42 is required for the shmoo formation but not for the MAPK^{Spk1} activation

During the vegetative cycle, *ras1Δ* cells show spherical cell morphology (Fukui et al., 1986; Nadin-Davis et al., 1986a) and polarised localisation of active Cdc42 is compromised (Kelly and Nurse, 2011), (Fig. 4C, D), indicating that Ras1 is involved in Cdc42 activation. The GTP-loaded Cdc42 is then predicted to activate the downstream Ste20-like kinase, Pak1/Shk1 (Endo et al., 2003; Marcus et al., 1995; Ottilie et al., 1995; Verde et al., 1995), resulting in actin reorganisation and shmoo formation under mating conditions (Bendezu and Martin, 2013; Merlini et al., 2016).

To confirm that Cdc42 acts downstream of Ras1, we generated a double mutant strain harbouring *ras1.G17V* and deletion of *scd1*, encoding a GDP-GTP exchanging factor for Cdc42 (Cdc42-GEF^{Scd1}). The *ras1.G17V* elongated shmoo phenotype was lost in the double mutant and instead, the cells showed a mating-deficient phenotype similar to the *cdc42-GEF^{scd1}Δ* single mutant (Fig 3A). The result supports the model that Cdc42 acts downstream of Ras1 to cause morphological changes.

Intriguingly, in the strains harbouring the *cdc42-GEF^{scd1}Δ* mutation, a nuclear MAPK^{Spk1}-GFP signal appeared (Fig. 3A), indicating that activation of MAPK^{Spk1} may not be impaired by lack of active Cdc42. This was unexpected because in a previous study, it was predicted that activation of Cdc42 contributes to activation of MAPKKK^{Byr2} (Tu et al., 1997). To clarify this issue, we measured **pp**MAPK^{Spk1} in the *cdc42-GEF^{scd1}Δ* mutant. Strikingly, in these cells MAPK^{Spk1} activation occurred with a reproducible advancement of the initial activation timing compared to the wildtype cells (Fig. 3B). The result shows that MAPK^{Spk1} activation does not require Cdc42 activity. Additionally, the faster activation of MAPK^{Spk1} raises the interesting possibility that two Ras1 effectors, MAPKKK^{Byr2} and Cdc42-GEF^{Scd1}, are competing with each other for activated Ras1, thus, lack of Cdc42-GEF^{Scd1} results in an advanced MAPK^{Spk1} activation (modelled in Fig. 7A).

Substantial MAPK^{Spk1} activation in the *cdc42-GEF^{scd1}Δ* mutant means that the mating deficiency of this mutant is unlikely to be the result of the lack of MAPK^{Spk1} activation. Indeed, introduction of *MAPKK$^{byr1.DD}$* to the *cdc42-GEF^{scd1}Δ* mutant did not restore the mating deficient phenotype, even though nuclear MAPK^{Spk1}-GFP highly accumulated (Fig. 3C). The result shows that active Cdc42 function is absolutely required for the mating process regardless of the MAPK^{Spk1}

activation status. Taken together with the essential role of MAPK^{Spk1}, we concluded that the mating pheromone signalling feeds into at least two pathways, MAPK^{Spk1} and Cdc42.

(6) Ras1 activates two effector pathways, MAPK^{Spk1} and Cdc42.

In order to further clarify the role of Ras1 we examined the MAPK^{Spk1} activation status and cell morphology in the following four strains: *ras1Δ* mutant, *ras1Δ MAPKK$^{byr1.DD}$* double mutant, *MAPKKK^{byr2}Δ* mutant and *MAPKKK^{byr2}Δ MAPKK$^{byr1.DD}$* double mutant. As mentioned earlier, deletion of *ras1* causes cells to show a round morphology (Fig. 3F), with reduced cortical signal of CRIB-GFP, an indicator of the active GTP-bound form of Cdc42, showing that Cdc42 activation is compromised (Fig.4C, D). *ras1* deletion also causes substantial reduction, but not complete elimination, of the **pp**MAPK^{Spk1} (Fig. 3D, red line, and Supplementary Fig. S3A); thus, Ras1 plays an important role in activating both Cdc42 and MAPK^{Spk1} pathways. Introduction of the *MAPKK$^{byr1.DD}$* mutation into the *ras1Δ* mutant cells induces the constitutive **pp**MAPK^{Spk1} (Fig. 3D, green line and Supplementary Fig. S3A) but does not affect the round cell morphology and cells remain sterile (Fig. 3F, the 2nd left panel. Note the accumulating MAPK^{Spk1}-GFP at 16 hours after induction of mating), as was the case for the *Cdc42-GEF^{Scd1}Δ MAPKK$^{byr1.DD}$* double mutant (Fig. 3C).

In a striking contrast, the sterile phenotype of the *MAPKKK^{byr2}Δ*, associated with complete lack of shmoo formation (Fig. 3F, the 2nd right panel), was converted to the "*fus*" phenotype, when combined with the *MAPKK$^{byr1.DD}$* mutation (Fig. 3F, the far right panel). As expected, the *MAPKKK^{byr2}Δ MAPKK$^{byr1.DD}$* double mutant shows MAPK^{Spk1} constitutive activation (Fig. 3E and Supplementary Fig. S3B). Thus, unlike the cases of *scd1Δ* or *ras1*Δ, lack of *MAPKKK^{byr2}* can be bypassed by constitutive activation of MAPK^{Spk1}, indicating that the sole role of MAPKKK^{Byr2} is to activate the MAPK^{Spk1} unlike its upstream activator, Ras1, which also activates Cdc42 pathway (a model presented in Fig. 7A).

(7) Ras1.G17V causes accumulation of Cdc42-GTP at the cell cortex.

Having observed a relatively mild influence of Ras1.G17V towards the MAPK^{Spk1} activation, we next examined whether the Cdc42 pathway was affected by the *ras1.G17V* mutation. We visualized the active GTP-bound form of Cdc42 (Cdc42^{GTP}) using CRIB-GFP that specifically binds to Cdc42^{GTP} (Tatebe et al., 2008). As previously observed, dynamic foci of CRIB-GFP appeared on the cell cortex upon induction of mating (Bendezu and Martin, 2013)(Fig. 4A and B). In our

experimental condition, more than 80% of wildtype cells showed the cortical CRIB-GFP signal at 4.5 hours after induction of mating (Fig. 4B). The cortical CRIB-GFP foci became concentrated at the site of mating and quickly disappeared once cells fused successfully to form zygotes (Fig. 4A and B). In striking contrast, in the *ras1.G17V* mutant cells, the cortical CRIB-GFP signal persisted, often at the elongated tip end of the cells, even 12.5 hours after induction of mating (Fig. 4A and B). The signal could still be seen in about 40% of the cells 22.5 hours after induction of mating (Fig. 4A and B). The result shows that the Cdc42 pathway is excessively activated in the *ras1.G17V* mutant and the localisation pattern of $Cdc42^{GTP}$ indicates that the signature "elongated" *ras1.G17V* morphological phenotype is caused by deregulation of the Cdc42 pathway.

Ras1-mediated Cdc42 pathway activation has been also indicated during the vegetative growth where the *ras1⊿* mutant shows a round cell morphology (Chang et al., 1994; Kelly and Nurse, 2011). However, unlike during the mating process, the *ras1.G17V* mutation does not cause an obvious morphological phenotype during the vegetative growth. We predicted that, during the vegetative growth, rigorous negative regulation occurs for Cdc42 by GTPase activation protein(s) (GAPs), such as Rga4 (Das et al., 2007; Kelly and Nurse, 2011; Tatebe et al., 2008) to counteract the effect of *ras1.G17V*. To examine this possibility, we compared Cdc42 activation status of vegetatively growing wildtype, *ras1*Δ, *ras1.G17V*, *rga4Δ*, and *rga4Δ ras1.G17V* double mutant cells (Fig. 4C and D). As previously described, CRIB-GFP showed a clearly polarized signal at the growing cell tips in the wildtype strain (Tatebe et al., 2008)(Fig. 4C and D). In the *ras1*Δ mutant, the cells were round and CRIB-GFP signal on the cell cortex had largely disappeared as was seen in the *cdc42-GEF^{scd1}*Δ mutant (Kelly and Nurse, 2011). In contrast, the cortical CRIB-GFP signal was clearly increased in the *ras1.G17V* single mutant although the cell morphology appeared largely similar to the wildtype cells (Fig. 4C, D). These results indicate a direct involvement of Ras1 in activating Cdc42. Meanwhile, the *rga4Δ* mutant cells showed slight alterations to the cell morphology, accompanied with less polarized distribution of cortical CRIB-GFP signal, as has been reported (Fig. 4C and D) (Das et al., 2007; Kelly and Nurse, 2011; Tatebe et al., 2008). Strikingly, the *rga4Δ ras1.G17V* double mutant showed a clear morphological alteration (big round cells) and the strongest cortical CRIB-GFP signal among all the mutants examined (Fig. 4C and D). The result fits well with our hypothesis that Ras1.G17V is activating Cdc42 even during vegetative growth, but the overall effect of Ras1.G17V is counteracted by the Cdc42-GAP, Rga4.

(8) Ras1 and an adaptor protein Ste4 are both necessary to fully activate MAPKKK^{Byr2}

Although Ras1 clearly plays the major role to activate MAPK^{Spk1}, a marginal, but detectable level of **pp**MAPK^{Spk1} was still induced in the *ras1Δ* mutant (Fig. 3D and Supplementary Fig. S3A), indicating that there is a Ras1-independent mechanism to activate MAPK^{Spk1}. Previous studies proposed an adaptor protein, Ste4, to be involved in the activation of MAPKKK^{Byr2}(Barr et al., 1996; Okazaki et al., 1991; Ramachander et al., 2002; Tu et al., 1997). We therefore examined whether Ste4 is required for MAPK^{Spk1} activation.

In constrast to the *ras1Δ* mutant, we detected virtually no MAPK^{Spk1} phosphorylation in the *ste4Δ* mutant (Fig. 5A and Supplementary Figure S3C), indicating that the adaptor^{Ste4} is a prerequisite for the MAPK^{Spk1} activation and the **pp**MAPK^{Spk1} signal observed in the *ras1Δ* mutant is dependent on Ste4 function. Introduction of *ras1.G17V* mutation neither restored the MAPK^{Spk1} activation nor mating (Fig. 5A, B), thus, activation of Ras1 cannot take over Ste4 function. In a striking contrast, the *ste4Δ MAPKK$^{byr1.DD}$* double mutant showed the *"fus"* phenotype as the *MAPKK$^{byr1.DD}$* single mutant cells and induced constitutive MAPK^{Spk1} activation, indicating that Ste4 is solely required for MAPK^{Spk1} activation (Fig. 5A, B).

Taken together, MAPKKK^{Byr2} is activated through a mechanism involving both Ras1 and Ste4, but Ste4 only conveys the signal towards the MAPK^{Spk1}, while Ras1 also activates Cdc42.

(9) Ste6, a Ras1 GTP-GDP exchange factor, contributes to both the MAPK^{Spk1} and the Cdc42 pathway activation

There are two GDP-GTP exchange factors (GEFs) identified for Ras1: Ste6 and Efc25 (Hughes et al., 1990; Tratner et al., 1997). As to the functional differences, Ste6 is essential for mating but is dispensable during the vegetative cycle whilst Efc25 is dispensable for mating but is required to maintain the cell morphology during the vegetative growth (Hughes et al., 1990; Tratner et al., 1997). There has been an interesting proposition that Ste6 may specifically help Ras1 to activate the MAPK^{Spk1} pathway, but not the Cdc42 pathway, whilst Efc25 specifically facilitates Ras1 to activate the Cdc42 pathway (Papadaki et al., 2002). We examined this hypothesis by monitoring the MAPK^{Spk1} activation status and conducting genetic epistasis analysis of *ras1.G17V* and *MAPKK$^{byr1.DD}$* in the *ste6Δ* mutant.

In *ste6Δ* cells, MAPK^{Spk1} phosphorylation was found somewhat reduced but occurred at a clearly detectable level. The signal increased when the *ras1.G17V* mutation was introduced (Fig. 5C and

Supplementary Figure S3D). When *ste6Δ and MAPKK$^{byr1.DD}$* were combined, MAPK^{Spk1} signalling recapitulated the *MAPKK$^{byr1.DD}$* activation profile (Fig. 5C and Supplementary Figure S3D). Nonetheless, the "pheromone-insensitive sterile" morphology of *ste6Δ* was only rescued by *ras1.G17V*, as previously reported, exhibiting the "elongated" phenotype (Hughes et al., 1990), but not by MAPKK$^{byr1.DD}$ (Fig. 5D). The result indicates that, unlike *ste4Δ* mutant, the mating deficiency of *ste6Δ* is not caused by mere lack of MAPK^{Spk1} activation but by lack of Ras1 activation. We concluded that Ste6 functions to activate Ras1, which then activates *both* the MAPK and Cdc42 pathways in response to pheromone signalling.

(10) Activation mutant of Gpa1 mimics the full pheromone signalling

In order to generate an integrated prototype Ras signalling model, we further investigated the upstream signal input machinery. Previous studies showed that Gpa1 plays the primary role in pheromone signalling (Obara et al., 1991). In agreement, in the *gpa1Δ* mutant we detected no MAPK^{Spk1} activation nor nuclear accumulation of MAPK^{Spk1}-GFP (Fig. 6A, B and Supplementary Fig. S4A). Introducing the *ras1.G17V* to the *gpa1Δ* strain did not rescue the complete lack of *MAPK^{Spk1}* activation nor did it induce a shmoo-like morphological change (Fig. 6A, B and Supplementary Fig. S4A), supporting our earlier observation that a Ras1-independent mechanism, involving Ste4 is essential for MAPK^{Spk1} activation. Meanwhile, introducing the *MAPKK$^{byr1.DD}$* mutation caused the constitutive activation of MAPK^{Spk1} (Fig. 6A and Supplementary Fig. S4A), but cells showed no morphological change (Fig. 6B). When both *ras1.G17V* and *MAPKK$^{byr1.DD}$* mutations were introduced into the *gpa1Δ* strain, MAPK^{Spk1} was activated and a shmoo-like morphological change occurred (Fig. 6A, B and Supplementary Fig. S4A). Therefore, activation of both of these two molecules is required and sufficient to mimic the pheromone signalling.

To further confirm that the Gpa1 is a central component of pheromone signalling, we looked into the MAPK^{Spk1} activation status in the constitutively active *gpa1.QL* mutant, which exhibits a "shmoo-like" morphological change in the heterothallic *h$^-$* strain without the mating partner (Obara et al., 1991).

Upon nitrogen starvation, the *h$^-$ gpa1.QL* mutant strain showed morphological changes and a strong MAPK^{Spk1} activation (Fig. 6C red line, Fig. 6D and Supplementary Fig. S4B). This response was largely dependent on the Ras1 function as the *h$^-$ gpa1.QL ras1Δ* double mutant exhibited a significantly reduced level of **pp**MAPK^{Spk1} and a round cell morphology, two typical features of

ras1Δ cells (Fig. 6C, D and Supplementary Fig. S4B). On the other hand, the *h⁻ ras1.G17V* single mutant showed a very low level of MAPK^{Spk1} activation, comparable to the one observed in the *h⁻* wildtype strain, with no apparent morphological alternation, confirming that sole activation of Ras1 does not substitute the pheromone signalling.

The *h⁻ MAPKK$^{byr1.DD}$* mutant induced a strong constitutive MAPK^{Spk1} activation, confirming that the MAPKK$^{Byr1.DD}$ molecule can activate MAPK^{Spk1} regardless of the pheromone signal input (Fig. 6C, light-blue line and Supplementary Fig. S4B). However, cell morphology was unchanged (Fig. 6D). Collectively, these results support the model where Gpa1 acts as the central transducer of the pheromone signalling, which can be mimicked only if both MAPK^{Spk1} and Ras1 are activated.

(11) A holistic modelling framwork of MAPK^{Spk1} activation

Based on quantitative **pp**MAPK^{Spk1} measurements in wildtype and various mutant strains (Fig. 1C, E, G, and Fig. 3B), we constructed a mathematical model of the MAPK^{Spk1} signalling dynamics. The aim of the model is to test whether a simple competition of the MAPK and the Cdc42 pathways for a shared pool of active Ras^{GTP}, can explain why the *scd1Δ* strain shows the similar **pp**MAPK^{Spk1} activation profile as the *ras1.G17V* strain.

We designed a reductionist model of 6 ordinary differential equations to represent key steps of pheromone signalling (Fig. 7A, Supplementary Fig. S5 and materials and methods). Model simulations and parameter estimations were performed in COPASI (Hoops et al., 2006) and details of the modelling process are described in Materials and Methods. Each biochemical process is referred as [L1]-[L10] as depicted in Fig. 7A. The signalling components were set to interact without delay based on the observations that signalling components are localized in close proximity (Fig. 1 and Fig. 4)(Dudin et al., 2016; Merlini et al., 2016; Merlini et al., 2018).

The framework of the modelling process is as follows: Genes encoding pheromones, receptors, Gpa1, Ste4 and Ste6 are all known to be under regulation of Ste11, the master transcriptional regulator for meiotic genes (Hughes et al., 1994; Mata and Bahler, 2006; Mata et al., 2002; Mata et al., 2007; Sugimoto et al., 1991) and these components are grouped into the Pheromone Sensing (PS) unit. During the vegetative growth, the PS unit is set to zero. Nitrogen starvation activates Ste11 (Kjaerulff et al., 2007; Sugimoto et al., 1991), which induces the PS unit [L1]. The PS unit activates MAPKKK^{Byr2} in a twofold manner: Directly by Ste4 [L3] and through Ras1 [L4](Fig. 7A). Activated MAPKKK^{Byr2} then triggers activation of MAPKK^{Byr1} [L5] that activates

MAPK^{Spk1} [L6]. Since activated MAPK^{Spk1} further activates Ste11 (Kjaerulff et al., 2005), MAPK^{Spk1} has a positive feedback loop on its own expression via Ste11 [L2,L7] (Fig. 7A).

As the pheromone signalling was found to induce a transient **pp**MAPK^{Spk1} peak (Fig. 1C), **pp**MAPK^{Spk1} activity is ought to be regulated by a delayed downregulation. Because the *MAPKK$^{byr1.DD}$* mutant completely lacks downregulation (Fig. 1E), downregulation occurring downstream of MAPKK^{byr1} (e.g.: Pyp1 and Pmp1) were considered physiologically insignificant. Meanwhile, Sxa2 (a serine carboxypeptidase against a mating pheromone P-factor) and Rgs1 (a regulator of Gpa1), both of which are induced upon successful pheromone signalling (Imai and Yamamoto, 1992; Mata and Bahler, 2006; Pereira and Jones, 2001; Watson et al., 1999), receptor internalization (Hirota et al., 2001) and regulation of the *mapk^{spk1}* transcript or other components by antisense RNA (Bitton et al., 2011) fit well to the criteria for the negative feedback. We represented all these potential negative feedbacks collectively as a single circuit, [L8]. Importantly, this downregulation [L8] works unperturbed in the presence of Ras1.G17V, by acting through the Ste4-dependent MAPKKK^{Byr2} activation process (Fig. 1G, Fig. 7A).

Ras1-GTP activates both the MAPKKK^{Byr2} and the Cdc42 pathways [L9] (Chang et al., 1994). As opposed to previous expectations that active Cdc42^{GTP} is required to activate MAPKKK^{Byr2} (Tu et al., 1997), deletion of Cdc42-GEF^{Scd1} does not compromise MAPK^{Spk1} activation (Fig. 3B) and rather, it makes **pp**MAPK^{Spk1} dynamics remarkably similar to that of the Ras1.G17V strain (Fig. 3B and Fig. 1G, plotted together in Fig. 7B): in both cases, **pp**MAPK^{Spk1} peaks earlier than the wildtype case. At a molecular level, reactions depleting the Ras1^{GTP} pool are compromised in both strains. Therefore, to explain these observations, we hypothesized that MAPK^{Spk1} and Cdc42 pathways are competing for the common Ras1^{GTP} pool. In this manner, one of the pathways can modulate the other by changing the amount of unbound (available) Ras1^{GTP}.

In support of this prediction, we showed that binding of recombinant Ras1.G17V^{GTP} to a MAPKKK^{Byr2} fragment was reduced by the presence of a Cdc42-GEF^{Scd1} fragment *in vitro* (Fig. 7C, D). In this assay, bacterially expressed GST tagged fragments of both MAPKKK^{Byr2} (65-180) and Cdc42-GEF^{Scd1} (760-872) showed a specific binding towards the GTP-loaded Ras1.G17V (1-172) (Fig. 7C). However, the binding of Ras1.G17V^{GTP} to MAPKKK^{Byr2} was substantially decreased when the Cdc42-GEF^{Scd1} fragment was added (Fig. 7D). The result likely refects the intrinsic biochemical competitive nature of MAPKKK^{Byr2} and Cdc42-GEF^{Scd1} for Ras1 binding. As we show below, this simple hypothesis successfully describes pheromone signalling mutants tested in this

study, suggesting that no unproven cross links are necessary to reproduce the *in vivo* observations.

An intriguing common feature observed in both Cdc42-GEF^{scd1}Δ and *ras1.G17V* mutants is that **pp**MAPK^{Spk1} peaks not only at an earlier time point, but also with a *lower amplitude* as compared to the wildtype. If increased Ras1^{GTP} levels simply accelerate MAPK^{Spk1} activation, as has been conventionally assumed, **pp**MAPK^{Spk1} production should peak earlier *and higher* (Supplementary Fig S6B, best fit out of 1000 global fits), and the addition of Ras1^{GTP} only should increase the amplitude, but not affect timing (Supplementary Fig S6C). We confirmed these results in the best models from 1000 global fits (Materials and Methods). The comparison between our experimental results and the *in silico* predictions suggests that the role of Ras1^{GTP} is more complex than previously thought.

Strikingly, if we hypothesize that Ras1^{GTP} also contributes to the negative feedback [L10] (Fig. 7A), we recapitulate the "*earlier and lower*" peak of **pp**MAPK^{Spk1} in both the *ras1.G17V* and the Cdc42-GEF^{scd1}Δ mutants (Fig. 7B). We currently do not have a direct experimental evidence to support [L10]. However, considering the fact that Ras1^{GTP} likely acts as a physical signalling hub at the cell cortex, mediating MAPKKK^{Byr2} recruitment and activation, which leads to recruitment of MAPKK^{Byr1} and MAPK^{Spk1}, Ras1^{GTP} may work as a two-way amplifier, both assisting localized MAPK^{Spk1} activation at the shmoo site, as well as helping the negative feedback by concentrating the affected molecules.

The model successfully recapitulated the experimental results for wildtype, *ras1.G17V*, MAPKK$^{Byr1.DD}$ and *cdc42-GEF^{scd1}Δ* mutants (Fig. 7B). To test the predictive capacity of the model, we next performed an *in silico* experiment where we titrated increasing amounts of Ras1^{GTP} in the wildtype condition before nitorgen removal. In agreement with our hypothesis, we obtained a *ras1.G17V*-like **pp**MAPK^{Spk1} activation profile with increasing amount of Ras1^{GTP}, i.e., the **pp**MAPK^{Spk1} peaks earlier with a lower peak intensity (Fig. 7E). The result further supported that Ras1^{GTP} availability alone is sufficient to explain both the *ras1.G17V* and *Cdc42-GEF^{scd1}Δ* phenotypes.

To further test the predictive value of the model, we asked whether it could predict **pp**MAPK^{Spk1} dynamics in the 21 other strains, which were measured (Fig. 2-6), but not used for fitting the model. We implemented each mutation in the wildtype model (Supplementary Table S2) and the model accurately predicted relative **pp**MAPK^{Spk1} dynamics in 17 cases, or showed predicitons in close proximity to the observed **pp**MAPK^{Spk1} dynamics in the 4 remaining cases

(Fig. 7F). Concluding from these results, our model likely represents the physiological framework of fission yeast RAS-MAPK signalling.

Discussion

By quantitating the $MAPK^{Spk1}$ and Cdc42 activation status during the mating process and conducting epistasis analysis between numerous signalling mutants, we showed that Ras1 coordinates activation of both the $MAPK^{Spk1}$ cascade and the Cdc42 pathway. Furthermore, we revealed that the *ras1.G17V* mutant phenotype is caused by deregulation of Cdc42, rather than altered activation of $MAPK^{Spk1}$ in physiological setting. Based on the experimental data, we built a mathematical model, which hypothesize that the $MAPK^{Spk1}$ cascade is subject to robust feedback regulation and two Ras1 effectors, Cdc42-GEF^{Scd1} and $MAPKKK^{Byr2}$, are competing for active Ras1. This model faithfully recapitulates $MAPK^{Spk1}$ activation profiles in the wildtype and all mutant strains examined in this study. The model implies that targeting one of the RAS effector pathways can potentially result in a complex outcome, rather than simply shutting down the targeted effector pathway. We concluded that fission yeast pheromone Ras signalling is not only defined by compartmentalisation (Onken et al., 2006) but rather a coordination of events involving both the $MAPK^{Spk1}$ and Cdc42 pathways.

In this study, we confirmed that Gpa1 is the central player of the pheromone signalling. It is likely that Gpa1 is the most downstream molecule conveying the complete pheromone signal. Considering that all the pheromone signalling components examined so far have been found at the shmoo site (Dudin et al., 2016; Merlini et al., 2016; Merlini et al., 2018)(this study), an attractive hypothesis is as follows: firstly, the activated pheromone receptor Map3/Mam2 locally activates Gpa1, which activates Ras1 and $MAPK^{Spk1}$. This then leads to a localised activation of the Cdc42, causing shmoo formation in the direction of a mating partner (Fig. 7G). The *ras1.G17V* mutation led to a acute activation of $MAPK^{Spk1}$ compared with the wildtype cells. The G17V mutantion of Ras1 is equivalent of G12V mutation of mammalian RAS, which results in a substantial reduction of both intrinsic and GAP-mediated GTPase activities (Trahey and McCormick, 1987). Therefore a larger fraction of Ras1 is expected to be in the GTP-bound form in the *ras1.G17V* mutant cells. By mathematical modelling, we showed that the increased $Ras1^{GTP}$ pool can explain a faster acute activation of $MAPK^{Spk1}$.

To our surprise, the constitutive Ras1.G17V mutation did not induce over-activation of MAPK^{Spk1}. The attenuated MAPK^{Spk1} activation in the presence of Ras1.G17V indicated that an efficient feedback mechanism is in place to counteract the effect of Ras1.G17V. Strikingly, the same trend has been reported in the mouse model of the *K-ras^{G12D}* mutation integrated at the endogenous chromosome locus (Tuveson et al., 2004). Therefore it is highly likely that the MAPK cascade is generally robust against upstream oncogenic constitutive stimulation.

Based on our observation that the MAPK^{Spk1} is constitutively activated in the *MAPKK$^{byr1.DD}$* mutant, we predict that the negative regulation occurs upstream of, or at the same level as, MAPKK^{Byr1}, rather than phosphatases that directly regulate MAPK^{Spk1}. In humans, ERK is shown to phosphorylate RAF proteins, the prototype MAPKKKs, to contribute to ERK signal attenuation (Brummer et al., 2003; Dougherty et al., 2005; Ritt et al., 2010). In future studies it will be important to determine whether MAPK^{Spk1} can directly downregulate MAPKKK^{Byr2} in a physiological setting.

Our results also show that an adaptor^{Ste4} plays a crucial role in activating MAPKKK^{Byr2}, abolishing **pp**MAPK^{Spk1} production even in the presence of *ras1.G17V* mutation. This suggests that the adaptor^{Ste4} fits well to be one of the major targets by the negative feedback loop against **pp**MAPK^{Spk1}. This mechanism is shared by budding yeast, where an adaptor protein, Ste50, modulates MAPKKK^{Ste11} (Ramezani-Rad, 2003). In humans, although such an adaptor protein for RAF proteins has yet to be identified, multiple RAF-interacting proteins, including 14-3-3 proteins, as well as formation of heterodimers between BRAF and CRAF, have been studied for their Ras-independent mechanism to activate RAF proteins (Lavoie and Therrien, 2015). Collectively, MAPK cascades seem to retain a general resistance to oncogenic RAS mutations in physiological settings.

Whilst lack of Cdc42 activation does not impair MAPK^{Spk1} activation, we found that MAPK^{Spk1} activity is required for shmoo formation even in the presence of Ras1.G17V (Fig. 2C). Therefore, the two Ras1 effectors, Cdc42 and MAPK^{Spk1} pathways, are not completely separable. The situation is reminiscent of the *K-ras^{G12D}* MEFs (Tuveson et al., 2004). In this system, the *K-ras^{G12D}* MEFs showed morphological anomalies. As both ERK and AKT phosphorylation levels in the *K-ras^{G12D}* MEFs resembled wildtype, these pathways unlikely caused the morphological phenotype. Nonetheless, inhibitors against MAPK and PI3K pathways reverted the *K-ras^{G12D}*–induced abnormal morphology back to the one similar to wildtype. The observation suggests that MAPK and PI3K pathways somehow contribute to the *K-ras^{G12D}* morphological phenotype;

for example, a basal level of MAPK and PI3K pathway activation may be a prerequisite for the *K-ras*^{G12D}–induced morphological anomalies.

The molecular mechanism of how MAPK^{Spk1} contributes to Cdc42 activation will require further studies. Key components in pheromone signalling are transcriptionally up-regulated upon pheromone signalling (Xue-Franzen et al., 2006). This is driven by MAPK^{Spk1}, which activates the master transcriptional regulator Ste11 (Kjaerulff et al., 2005; Mata and Bahler, 2006; Xue-Franzen et al., 2006). Therefore, the contribution of MAPK^{Spk1} to Cdc42 activation is expected to occur, at least partly, through transcriptional activation.

In addition, localisation of signalling components may be regulated by MAPK^{Spk1}. In budding yeast, Cdc24, the GEF for Cdc42, is sequestered into the nucleus by an adaptor protein Far1 (Nern and Arkowitz, 2000; Shimada et al., 2000). Upon the pheromone signalling, budding yeast MAPK^{Fus3} phosphorylates Far1, which then brings Cdc24 out to the shmoo site, leading to Cdc42 activation on the cell cortex (Hegemann et al., 2015).

MAPK^{Spk1} may also directly phosphorylate to activate Cdc42 and/or its regulatory proteins such as Cdc42-GEF^{Scd1}, Scd2 or GAP-Cdc42^{Rga4}, all of which function at the shmoo site during the mating (Bendezu and Martin, 2013; Dudin et al., 2016)(Fig.4 A and B). In agreement with this hypothesis, a transient MAPK^{Spk1} and MAPKK^{Byr1} signal on the cell cortex was observed during the mating process (Fig. 1)(Dudin et al., 2016). Localisation of MAPK at the growing cell tips was also observed in other fungi including *S. cerevisiae* and *N. crassa* (Chen et al., 2010; Fleissner et al., 2009; Maeder et al., 2007; van Drogen et al., 2001). In budding yeast, MAPK^{Fus3} can directly phosphorylates Bni1, a formin that organises actin filaments, to facilitate shmoo formation (Matheos et al., 2004).

Interestingly, during the vegetative growth when expression of MAPK^{Spk1} is repressed, Ras1.G17V is still capable of activating Cdc42 (Fig. 4C and D). Whether other MAPKs, such as Sty1 or Pmk1, contribute to Cdc42 activation during the vegetative cell cycle will be an important question to answer. Intriguingly, recent studies show that Sty1 inhibits, rather than assists, establishment of the Cdc42 polarity module (Mutavchiev et al., 2016). Collectively, it is likely that the Cdc42 polarity module is regulated in a context dependent manner by multiple MAPKs in a range of ways.

In this study we revealed the vital contribution of Cdc42 to induce the *ras1.G17V* phenotype in fission yeast pheromone signalling. In mouse models, small GTPases, Cdc42 and Rac, are required for *H-ras*^{G12V} induced transformation (Malliri et al., 2002; Stengel and Zheng, 2012).

Therefore, oncogenic RAS-induced Cdc42/Rac misregulation may be a common basis of oncogenicity of mutated-RAS-induced signalling. Specifically targeting this process may therefore be an effective strategy against oncogenic RAS-driven tumourigenesis.

Acknowledgment

The authors thank Tatsuya Maeda, Thibault Mayor, Janni Petersen, Louise Fairall, John Schwabe, David Critchley, Andrey Reviyakin, Gary Willars and Mohan Harihar for helpful suggestions, stimulating discussions and critical reading of the manuscript. We thank PROTEX and PNACL at University of Leicester for their technical assistance. We are grateful to Kazu Shiozaki, Keith Gull and Yeast Genetic Resource Center for providing strains and antibodies. This work was funded by the Wellcome Trust Institutional Strategic Support Fund WT097828/Z/11/Z, WT097828/Z/11/B and the Deutsche Forschungsgemeinschaft (DFG) EXC 81. A.V. was supported by German Academic Exchange Service (DAAD) A0981674.

Author Contributions

E.J.K., S.R. and K.T. generated yeast strains. E.J.K., G.S. and K.T. monitored activation status of $MAPK^{Spk1}$ and Cdc42. A.V. and E.K. conducted mathematical modelling. E.J.K., K.S. and K.T. conducted image analysis. M.T., R.G., C.P. and C.D. conducted biochemical analysis of Ras1, Byr2 and Scd1. E.J.K., A.V., E.K. and K.T. designed the experiments and interpreted the data.

Declaration of Interests

The authors declare no competing interests.

References

Barr, M.M., Tu, H., Van Aelst, L., and Wigler, M. (1996). Identification of Ste4 as a potential regulator of Byr2 in the sexual response pathway of Schizosaccharomyces pombe. Mol Cell Biol *16*, 5597-5603.

Bendezu, F.O., and Martin, S.G. (2013). Cdc42 explores the cell periphery for mate selection in fission yeast. Current biology : CB *23*, 42-47.

Bitton, D.A., Grallert, A., Scutt, P.J., Yates, T., Li, Y., Bradford, J.R., Hey, Y., Pepper, S.D., Hagan, I.M., and Miller, C.J. (2011). Programmed fluctuations in sense/antisense transcript ratios drive sexual differentiation in S. pombe. Mol Syst Biol *7*, 559.

589 Brummer, T., Naegele, H., Reth, M., and Misawa, Y. (2003). Identification of novel ERK-
590 mediated feedback phosphorylation sites at the C-terminus of B-Raf. Oncogene *22*, 8823-
591 8834.
592 Chang, E.C., Barr, M., Wang, Y., Jung, V., Xu, H.P., and Wigler, M.H. (1994). Cooperative
593 interaction of S. pombe proteins required for mating and morphogenesis. Cell *79*, 131-141.
594 Chen, R.E., Patterson, J.C., Goupil, L.S., and Thorner, J. (2010). Dynamic localization of Fus3
595 mitogen-activated protein kinase is necessary to evoke appropriate responses and avoid
596 cytotoxic effects. Mol Cell Biol *30*, 4293-4307.
597 Cox, A.D., and Der, C.J. (2010). Ras history: The saga continues. Small GTPases *1*, 2-27.
598 Das, M., Wiley, D.J., Medina, S., Vincent, H.A., Larrea, M., Oriolo, A., and Verde, F. (2007).
599 Regulation of cell diameter, For3p localization, and cell symmetry by fission yeast Rho-GAP
600 Rga4p. Molecular biology of the cell *18*, 2090-2101.
601 Didmon, M., Davis, K., Watson, P., Ladds, G., Broad, P., and Davey, J. (2002). Identifying
602 regulators of pheromone signalling in the fission yeast Schizosaccharomyces pombe.
603 Current genetics *41*, 241-253.
604 Dougherty, M.K., Muller, J., Ritt, D.A., Zhou, M., Zhou, X.Z., Copeland, T.D., Conrads, T.P.,
605 Veenstra, T.D., Lu, K.P., and Morrison, D.K. (2005). Regulation of Raf-1 by direct feedback
606 phosphorylation. Mol Cell *17*, 215-224.
607 Dudin, O., Merlini, L., and Martin, S.G. (2016). Spatial focalization of pheromone/MAPK
608 signaling triggers commitment to cell-cell fusion. Genes Dev *30*, 2226-2239.
609 Endo, M., Shirouzu, M., and Yokoyama, S. (2003). The Cdc42 binding and scaffolding
610 activities of the fission yeast adaptor protein Scd2. J Biol Chem *278*, 843-852.
611 Fleissner, A., Leeder, A.C., Roca, M.G., Read, N.D., and Glass, N.L. (2009). Oscillatory
612 recruitment of signaling proteins to cell tips promotes coordinated behavior during cell
613 fusion. Proceedings of the National Academy of Sciences of the United States of America
614 *106*, 19387-19392.
615 Fukui, Y., Kozasa, T., Kaziro, Y., Takeda, T., and Yamamoto, M. (1986). Role of a ras homolog
616 in the life cycle of Schizosaccharomyces pombe. Cell *44*, 329-336.
617 Fukui, Y., Miyake, S., Satoh, M., and Yamamoto, M. (1989). Characterization of the
618 Schizosaccharomyces pombe ral2 gene implicated in activation of the ras1 gene product.
619 Mol Cell Biol *9*, 5617-5622.
620 Gronwald, W., Huber, F., Grunewald, P., Sporner, M., Wohlgemuth, S., Herrmann, C., and
621 Kalbitzer, H.R. (2001). Solution structure of the Ras binding domain of the protein kinase
622 Byr2 from Schizosaccharomyces pombe. Structure *9*, 1029-1041.
623 Hegemann, B., Unger, M., Lee, S.S., Stoffel-Studer, I., van den Heuvel, J., Pelet, S., Koeppl, H.,
624 and Peter, M. (2015). A Cellular System for Spatial Signal Decoding in Chemical Gradients.
625 Dev Cell *35*, 458-470.
626 Hirota, K., Tanaka, K., Watanabe, Y., and Yamamoto, M. (2001). Functional analysis of the C-
627 terminal cytoplasmic region of the M-factor receptor in fission yeast. Genes Cells *6*, 201-
628 214.
629 Hoops, S., Sahle, S., Gauges, R., Lee, C., Pahle, J., Simus, N., Singhal, M., Xu, L., Mendes, P., and
630 Kummer, U. (2006). COPASI--a COmplex PAthway SImulator. Bioinformatics *22*, 3067-3074.
631 Hughes, D.A., Fukui, Y., and Yamamoto, M. (1990). Homologous activators of ras in fission
632 and budding yeast. Nature *344*, 355-357.
633 Hughes, D.A., Yabana, N., and Yamamoto, M. (1994). Transcriptional regulation of a Ras
634 nucleotide-exchange factor gene by extracellular signals in fission yeast. J Cell Sci *107 (Pt*
635 *12)*, 3635-3642.
636 Imai, Y., and Yamamoto, M. (1992). Schizosaccharomyces pombe sxa1+ and sxa2+ encode
637 putative proteases involved in the mating response. Mol Cell Biol *12*, 1827-1834.

638 Kelly, F.D., and Nurse, P. (2011). Spatial control of Cdc42 activation determines cell width in
639 fission yeast. Molecular biology of the cell *22*, 3801-3811.
640 Kjaerulff, S., Andersen, N.R., Borup, M.T., and Nielsen, O. (2007). Cdk phosphorylation of the
641 Ste11 transcription factor constrains differentiation-specific transcription to G1. Genes Dev
642 *21*, 347-359.
643 Kjaerulff, S., Lautrup-Larsen, I., Truelsen, S., Pedersen, M., and Nielsen, O. (2005).
644 Constitutive activation of the fission yeast pheromone-responsive pathway induces ectopic
645 meiosis and reveals ste11 as a mitogen-activated protein kinase target. Mol Cell Biol *25*,
646 2045-2059.
647 Lavoie, H., and Therrien, M. (2015). Regulation of RAF protein kinases in ERK signalling. Nat
648 Rev Mol Cell Biol *16*, 281-298.
649 Lin, A.W., Barradas, M., Stone, J.C., van Aelst, L., Serrano, M., and Lowe, S.W. (1998).
650 Premature senescence involving p53 and p16 is activated in response to constitutive
651 MEK/MAPK mitogenic signaling. Genes Dev *12*, 3008-3019.
652 Maeder, C.I., Hink, M.A., Kinkhabwala, A., Mayr, R., Bastiaens, P.I., and Knop, M. (2007).
653 Spatial regulation of Fus3 MAP kinase activity through a reaction-diffusion mechanism in
654 yeast pheromone signalling. Nat Cell Biol *9*, 1319-1326.
655 Malliri, A., van der Kammen, R.A., Clark, K., van der Valk, M., Michiels, F., and Collard, J.G.
656 (2002). Mice deficient in the Rac activator Tiam1 are resistant to Ras-induced skin tumours.
657 Nature *417*, 867-871.
658 Marcus, S., Polverino, A., Chang, E., Robbins, D., Cobb, M.H., and Wigler, M.H. (1995). Shk1, a
659 homolog of the Saccharomyces cerevisiae Ste20 and mammalian p65PAK protein kinases, is
660 a component of a Ras/Cdc42 signaling module in the fission yeast Schizosaccharomyces
661 pombe. Proceedings of the National Academy of Sciences of the United States of America *92*,
662 6180-6184.
663 Masuda, T., Kariya, K., Shinkai, M., Okada, T., and Kataoka, T. (1995). Protein kinase Byr2 is a
664 target of Ras1 in the fission yeast Schizosaccharomyces pombe. J Biol Chem *270*, 1979-
665 1982.
666 Mata, J., and Bahler, J. (2006). Global roles of Ste11p, cell type, and pheromone in the control
667 of gene expression during early sexual differentiation in fission yeast. Proceedings of the
668 National Academy of Sciences of the United States of America *103*, 15517-15522.
669 Mata, J., Lyne, R., Burns, G., and Bahler, J. (2002). The transcriptional program of meiosis
670 and sporulation in fission yeast. Nature genetics *32*, 143-147.
671 Mata, J., Wilbrey, A., and Bahler, J. (2007). Transcriptional regulatory network for sexual
672 differentiation in fission yeast. Genome biology *8*, R217.
673 Matheos, D., Metodiev, M., Muller, E., Stone, D., and Rose, M.D. (2004). Pheromone-induced
674 polarization is dependent on the Fus3p MAPK acting through the formin Bni1p. J Cell Biol
675 *165*, 99-109.
676 Merlini, L., Dudin, O., and Martin, S.G. (2013). Mate and fuse: how yeast cells do it. Open Biol
677 *3*, 130008.
678 Merlini, L., Khalili, B., Bendezu, F.O., Hurwitz, D., Vincenzetti, V., Vavylonis, D., and Martin,
679 S.G. (2016). Local Pheromone Release from Dynamic Polarity Sites Underlies Cell-Cell
680 Pairing during Yeast Mating. Current biology : CB *26*, 1117-1125.
681 Merlini, L., Khalili, B., Dudin, O., Michon, L., Vincenzetti, V., and Martin, S.G. (2018).
682 Inhibition of Ras activity coordinates cell fusion with cell-cell contact during yeast mating. J
683 Cell Biol *217*, 1467-1483.
684 Mutavchiev, D.R., Leda, M., and Sawin, K.E. (2016). Remodeling of the Fission Yeast Cdc42
685 Cell-Polarity Module via the Sty1 p38 Stress-Activated Protein Kinase Pathway. Current
686 biology : CB *26*, 2921-2928.

687 Nadin-Davis, S.A., and Nasim, A. (1988). A gene which encodes a predicted protein kinase
688 can restore some functions of the ras gene in fission yeast. EMBO J *7*, 985-993.
689 Nadin-Davis, S.A., Nasim, A., and Beach, D. (1986a). Involvement of ras in sexual
690 differentiation but not in growth control in fission yeast. EMBO J *5*, 2963-2971.
691 Nadin-Davis, S.A., Yang, R.C., Narang, S.A., and Nasim, A. (1986b). The cloning and
692 characterization of a RAS gene from Schizosaccharomyces pombe. J Mol Evol *23*, 41-51.
693 Nern, A., and Arkowitz, R.A. (2000). Nucleocytoplasmic shuttling of the Cdc42p exchange
694 factor Cdc24p. J Cell Biol *148*, 1115-1122.
695 Obara, T., Nakafuku, M., Yamamoto, M., and Kaziro, Y. (1991). Isolation and characterization
696 of a gene encoding a G-protein alpha subunit from Schizosaccharomyces pombe:
697 involvement in mating and sporulation pathways. Proceedings of the National Academy of
698 Sciences of the United States of America *88*, 5877-5881.
699 Okazaki, N., Okazaki, K., Tanaka, K., and Okayama, H. (1991). The ste4+ gene, essential for
700 sexual differentiation of Schizosaccharomyces pombe, encodes a protein with a leucine
701 zipper motif. Nucleic acids research *19*, 7043-7047.
702 Onken, B., Wiener, H., Philips, M.R., and Chang, E.C. (2006). Compartmentalized signaling of
703 Ras in fission yeast. Proceedings of the National Academy of Sciences of the United States of
704 America *103*, 9045-9050.
705 Ottilie, S., Miller, P.J., Johnson, D.I., Creasy, C.L., Sells, M.A., Bagrodia, S., Forsburg, S.L., and
706 Chernoff, J. (1995). Fission yeast pak1+ encodes a protein kinase that interacts with Cdc42p
707 and is involved in the control of cell polarity and mating. EMBO J *14*, 5908-5919.
708 Ozoe, F., Kurokawa, R., Kobayashi, Y., Jeong, H.T., Tanaka, K., Sen, K., Nakagawa, T., Matsuda,
709 H., and Kawamukai, M. (2002). The 14-3-3 proteins Rad24 and Rad25 negatively regulate
710 Byr2 by affecting its localization in Schizosaccharomyces pombe. Mol Cell Biol *22*, 7105-
711 7119.
712 Papadaki, P., Pizon, V., Onken, B., and Chang, E.C. (2002). Two ras pathways in fission yeast
713 are differentially regulated by two ras guanine nucleotide exchange factors. Mol Cell Biol *22*,
714 4598-4606.
715 Pereira, P.S., and Jones, N.C. (2001). The RGS domain-containing fission yeast protein,
716 Rgs1p, regulates pheromone signalling and is required for mating. Genes Cells *6*, 789-802.
717 Prior, I.A., Lewis, P.D., and Mattos, C. (2012). A comprehensive survey of Ras mutations in
718 cancer. Cancer Res *72*, 2457-2467.
719 Qiu, R.G., Abo, A., McCormick, F., and Symons, M. (1997). Cdc42 regulates anchorage-
720 independent growth and is necessary for Ras transformation. Mol Cell Biol *17*, 3449-3458.
721 Ramachander, R., Kim, C.A., Phillips, M.L., Mackereth, C.D., Thanos, C.D., McIntosh, L.P., and
722 Bowie, J.U. (2002). Oligomerization-dependent association of the SAM domains from
723 Schizosaccharomyces pombe Byr2 and Ste4. J Biol Chem *277*, 39585-39593.
724 Ramezani-Rad, M. (2003). The role of adaptor protein Ste50-dependent regulation of the
725 MAPKKK Ste11 in multiple signalling pathways of yeast. Current genetics *43*, 161-170.
726 Ritt, D.A., Monson, D.M., Specht, S.I., and Morrison, D.K. (2010). Impact of feedback
727 phosphorylation and Raf heterodimerization on normal and mutant B-Raf signaling. Mol
728 Cell Biol *30*, 806-819.
729 Schubbert, S., Bollag, G., and Shannon, K. (2007). Deregulated Ras signaling in
730 developmental disorders: new tricks for an old dog. Curr Opin Genet Dev *17*, 15-22.
731 Shimada, Y., Gulli, M.-P., and Peter, M. (2000). Nuclear sequestration of the exchange factor
732 Cdc24 by Far1 regulates cell polarity during yeast mating. Nature Cell Biology *2*, 117.
733 Sipiczki, M. (1988). The role of sterility genes (ste and aff) in the initiation of sexual
734 development in Schizosaccharomyces pombe. Molecular & general genetics : MGG *213*, 529-
735 534.

Stengel, K.R., and Zheng, Y. (2012). Essential role of Cdc42 in Ras-induced transformation revealed by gene targeting. PLoS One *7*, e37317.

Sugimoto, A., Iino, Y., Maeda, T., Watanabe, Y., and Yamamoto, M. (1991). Schizosaccharomyces pombe ste11+ encodes a transcription factor with an HMG motif that is a critical regulator of sexual development. Genes Dev *5*, 1990-1999.

Tatebe, H., Nakano, K., Maximo, R., and Shiozaki, K. (2008). Pom1 DYRK regulates localization of the Rga4 GAP to ensure bipolar activation of Cdc42 in fission yeast. Current biology : CB *18*, 322-330.

Toda, T., Shimanuki, M., and Yanagida, M. (1991). Fission yeast genes that confer resistance to staurosporine encode an AP-1-like transcription factor and a protein kinase related to the mammalian ERK1/MAP2 and budding yeast FUS3 and KSS1 kinases. Genes Dev *5*, 60-73.

Trahey, M., and McCormick, F. (1987). A cytoplasmic protein stimulates normal N-ras p21 GTPase, but does not affect oncogenic mutants. Science *238*, 542-545.

Tratner, I., FourticqEsqueoute, A., Tillit, J., and Baldacci, G. (1997). Cloning and characterization of the S-pombe gene efc25(+), a new putative guanine nucleotide exchange factor. Gene *193*, 203-210.

Tu, H., Barr, M., Dong, D.L., and Wigler, M. (1997). Multiple regulatory domains on the Byr2 protein kinase. Mol Cell Biol *17*, 5876-5887.

Tuveson, D.A., Shaw, A.T., Willis, N.A., Silver, D.P., Jackson, E.L., Chang, S., Mercer, K.L., Grochow, R., Hock, H., Crowley, D*., et al.* (2004). Endogenous oncogenic K-ras(G12D) stimulates proliferation and widespread neoplastic and developmental defects. Cancer Cell *5*, 375-387.

van Drogen, F., Stucke, V.M., Jorritsma, G., and Peter, M. (2001). MAP kinase dynamics in response to pheromones in budding yeast. Nat Cell Biol *3*, 1051-1059.

Verde, F., Mata, J., and Nurse, P. (1995). Fission yeast cell morphogenesis: identification of new genes and analysis of their role during the cell cycle. J Cell Biol *131*, 1529-1538.

Wang, Y., Xu, H.P., Riggs, M., Rodgers, L., and Wigler, M. (1991). byr2, a Schizosaccharomyces pombe gene encoding a protein kinase capable of partial suppression of the ras1 mutant phenotype. Mol Cell Biol *11*, 3554-3563.

Watson, P., Davis, K., Didmon, M., Broad, P., and Davey, J. (1999). An RGS protein regulates the pheromone response in the fission yeast Schizosaccharomyces pombe. Mol Microbiol *33*, 623-634.

Weston, C., Bond, M., Croft, W., and Ladds, G. (2013). The coordination of cell growth during fission yeast mating requires Ras1-GTP hydrolysis. PLoS One *8*, e77487.

Xu, H.P., White, M., Marcus, S., and Wigler, M. (1994). Concerted action of RAS and G proteins in the sexual response pathways of Schizosaccharomyces pombe. Mol Cell Biol *14*, 50-58.

Xue-Franzen, Y., Kjaerulff, S., Holmberg, C., Wright, A., and Nielsen, O. (2006). Genomewide identification of pheromone-targeted transcription in fission yeast. BMC Genomics *7*, 303.

Yamamoto, M. (1996). The molecular control mechanisms of meiosis in fission yeast. Trends Biochem Sci *21*, 18-22.

Zheng, C.F., and Guan, K.L. (1994). Activation of MEK family kinases requires phosphorylation of two conserved Ser/Thr residues. EMBO J *13*, 1123-1131.

Zhu, J., Woods, D., McMahon, M., and Bishop, J.M. (1998). Senescence of human fibroblasts induced by oncogenic Raf. Genes Dev *12*, 2997-3007.

Figure legends

Figure 1. Distinct modes of MAPK^{Spk1} temporal phosphorylation profile and morphological changes during sexual differentiation in wildtype, *MAPKK$^{byr1.DD}$* and *ras1.G17V* mutants.

(A) A pictorial representation of wildtype fission yeast sexual differentiation. (B) A list of key signalling components of the fission yeast pheromone signalling pathway. The diagram reflects the prediction that Gpa1 and Ras1 separately contribute to activation of MAPKKK^{Byr2} activation although the precise mechanism is unknown (Xu et al., 1994). At the same time, Ras1 activation is expected to be at least partly under influence of active Gpa1 because the *ste6* gene, encoding a Ras1 activator, is strongly induced upon successful pheromone signaling (Hughes et al., 1994). (C)-(H) Cells were induced for sexual differentiation by the plate mating assay system as described in the materials and methods. (C), (E) and (G) Quantified **pp**MAPK^{Spk1} signal from western blots of wildtype (KT3082) (C), *MAPKK$^{byr1.DD}$* (KT3435) (E) and *ras1.G17V* (KT3084) (G) cells. Three biological replicates were used for quantitation (error bars are ±SEM). α-tubulin was used as a loading control and quantitation was carried out using the Image Studio ver2.1 software (Licor Odyssey CLx Scanner). For the wildtype samples in (C), the % of cells mating is also indicated. The wildtype **pp**MAPK^{Spk1} result (C) is also presented in (E) and (G) as a reference. (D), (F) and (H) Cellular morphology (brightfield) and localization of MAPK^{Spk1}-GFP over a 24 hour time-course in wildtype (D), *MAPKK$^{byr1.DD}$* (F) and *ras1.G17V* (H) cells. Time after induction of mating in hours is indicated on the left. At each time point, a bright-field image and a GFP signal image were taken and processed as described in materials and methods. Green asterisks in the time 24 h in the *ras1.G17V* cell image (H) indicate auto-fluorescence signal from inviable cell debris, which were presumably produced through cytokinesis failure or cell lysis. Yellow arrows in panels (D) and (F) indicate transient accumulation of MAPK^{Spk1}-GFP at the shmoo tips. Scale bars represent 10µm.

Figure 2. In the *ras1.G17V MAPKK$^{byr1.DD}$* double mutant, the MAPK^{Spk1} phosphorylation profile follows *MAPKK$^{byr1.DD}$* single mutant phenotype whilst cell morphology mimics the *ras1.G17V* single mutant phenotype.

(A) MAPK^{Spk1} phosphorylation status in the *ras1.G17V MAPKK$^{byr1.DD}$* double mutant cells (KT3439). Cells were induced for mating by the plate mating assay system as described in the materials and methods. Quantitated **pp**MAPK^{Spk1} signal (arbitrary unit) from western blots is

presented. Results of two biological replicates (each derived from three technical replicates, error bars are ±SEM) are presented in red. (B) The terminal mating phenotype of *ras1.G17V MAPKK$^{byr1.DD}$* double mutant is a phenocopy of *ras1.G17V* single mutant which shows the "elongated" morphology. Images were taken of *ras1.G17V MAPKK$^{byr1.DD}$* double mutant (KT3439) in the same way as in Fig. 1. Time after induction of mating in hours is indicated on the left. (C) There is no morphological change in the absence of MAPK^{Spk1} signalling. Cell images of *MAPKK^{byr1}Δ* (KT4700) and *ras1.G17V MAPKK^{byr1}Δ* (KT5030) strains are shown. Images were taken in the same way as in Fig. 1. Time after induction of mating in hours is indicated on the left of each series. Scale bars represent 10µm.

Figure 3. Ras1 activates both MAPK^{Spk1} and Cdc42 pathways during pheromone signalling.

(A) *scd1Δ* morphology and MAPK^{Spk1}-GFP signal. Images of WT (KT3082), *scd1Δ* (KT4061) and *scd1Δ ras1.G17V* double mutant (KT4056) were taken in the same way as in Fig.1. Numbers on the left represents hours after induction of mating. (B) MAPK^{Spk1} phosphorylation state in *scd1Δ* (KT4061) cells after mating induction. Results of three biological replicates (error bars are ±SEM) are presented. The wildtype **pp**MAPK^{Spk1} result presented in Fig.1 (C) is also shown in blue as a reference. (C) Cell images of *scd1Δ MAPKK$^{byr1.DD}$* double mutant (KT4047) were taken in the same way as in Fig.1. Numbers on the left represents hours after induction of mating. (D) MAPK^{Spk1} phosphorylation state in *ras1Δ* (KT4323), *MAPKK$^{byr1.DD}$* (KT3435) and *ras1Δ MAPKK$^{byr1.DD}$* (KT4359) cell extracts. Original Western blotting data is presented in Fig. S3A. (E) MAPK^{Spk1} phosphorylation state in *mapkkk^{byr2}Δ* (KT3763), *MAPKK$^{byr1.DD}$* (KT3435) and *mapkkk^{byr2}Δ MAPKK$^{byr1.DD}$* (KT4010) cell extracts. Original Western blotting data is presented in Fig. S3B. For (D) and (E), quantification was carried out using the Image Studio ver2.1 (Li-cor). (F) Cell images of the strains mentioned in (D) and (E) were taken in the same way as in Fig.1. Numbers on the left represents hours after induction of mating. For all the images presented in (A), (C) and (F), scale bars represent 10µm.

Figure 4. Ras1.G17V induces cortical Cdc42^{GTP} accumulation

(A) Cell morphology and localisation of Cdc42^{GTP}, indicated by CRIB-GFP signal, during the sexual differentiation process. Wildtype (KT5077) and *ras1.G17V* (KT5082) mutant cells were induced for mating/sexual differentiation by the plate mating assay condition (Materials and Methods)

and live cell images were taken at the indicated time after induction of mating/sexual differentiation. Representative CRIB-GFP signal images are presented. Cells with cortical CRIB-GFP foci are indicated by orange stars. Rapidly-disappearing CRIB-GFP signals at the fusion site of wildtype mating cells are indicated by green arrows at time 8.5h image. Scale bar: 10 µm. (B) Quantitation of the results presented in (A). At each time point (4.5h, 6.5h, 10.5h, 12.5h and 22.5h after induction of mating/sexual differentiation), 150 cells were examined whether they have cortical CRIB-GFP foci. % cells with cortical CRIB-GFP foci is presented. The experiment was repeated for three times and the mean values and SDs are plotted in the graph. (C) Cell morphology and localisation of $Cdc42^{GTP}$, indicated by CRIB-GFP signal, during vegetative growth. Representative CRIB-GFP signal images of cells of wildtype (KT5077), *ras1Δ* (5107), *ras1.G17V* (KT5082), *rga4Δ* (5551) and *rga4Δ ras1.G17V* (KT5554) are presented. Scale bar: 10 µm. (D) Quantitated CRIB-GFP signals on the cell cortex of cells presented in (C). Intensity of GFP signal on the cell cortex was measured along one of the cell tips as indicated as a magenta dotted line in the example image on the right (Scale bar: 10 µm) as stated in the Materials and Methods. 40 cells without septum were measured for each strain and the average curve from all aligned traces per strain was calculated, and displayed with respective standard error of the mean curves (dashed lines) as described in Materials and Methods.

Fig. 5. Distinct contributions of Ste4 and Ste6 to $MAPK^{Spk1}$ phosphorylation.

(A) Ste4 is essential for $MAPK^{Spk1}$ activation. $MAPK^{Spk1}$ phosphorylation status in *ste4Δ* (KT4376), *ste4Δ ras1.G17V* (KT5143) and *ste4Δ* $MAPKK^{byr1.DD}$ (KT5136) at times-points 0, 8 ,16 and 24 hours post mating induction are presented. Original Western blotting membranes are presented in Fig. S3C. (B) Incapability of *ste4Δ* to cause pheromone-induced morphological change is suppressed by $MAPKK^{byr1.DD}$ but not by *ras1.G17V*. Cell images of *ste4Δ* (KT4376), *ste4Δ ras1.G17V* (KT5143) and *ste4Δ* $MAPKK^{byr1.DD}$ (KT5136) strains were taken 24 hours after induction of mating. Scale bar: 10 µm. (C) Lack of Ste6 does not result in the complete loss of $MAPK^{Spk1}$ phosphorylation. $MAPK^{Spk1}$ phosphorylation status in *ste6Δ* (KT4333), *ste6Δ ras1.G17V* (KT4998) and *ste6Δ* $MAPKK^{byr1.DD}$ (KT5139) at times-points 0, 8 ,16 and 24 hours post mating induction are presented. Original Western blotting membranes are presented in Fig. S3D. (D) Incapability of *ste6Δ* to cause pheromone-induced morphological change is suppressed by *ras1.G17V* mutation but not by $MAPKK^{byr1.DD}$ mutation. Cell images of *ste6Δ* (KT4333), *ste6Δ*

877 *ras1.G17V* (KT4998) and *ste6Δ MAPKK$^{byr1.DD}$* (KT5139) strains were taken 24 hours after
878 induction of mating. Scale bar: 10 µm.

879

880 **Fig. 6. Gpa1 transduces the pheromone signalling by activating MAPK^{Spk1} and Ras1 pathways**

881 (A) MAPK^{Spk1} phosphorylation status in homothallic *gpa1Δ* (KT4335), *gpa1Δ ras1.G17V*
882 (KT5023), *gpa1Δ MAPKK$^{byr1.DD}$* (KT4353) and *gpa1Δ ras1.val17 MAPKK$^{byr1.DD}$* (KT5035) at times-
883 points 0, 8 ,12, 16 and 24 hours after mating induction. Original Western membrane is
884 presented in Fig. S4A. (B) Cell images of the above mentioned strains at 16 hours after mating
885 induction. All the cell images were taken and processed as in Figure 1. Scale bar is 10 µm. (C)
886 MAPK^{Spk1} phosphorylation status in *h$^-$* WT (KT4190), *h$^-$ gpa1.QL* (KT5059), *h$^-$ ras1.G17V* (KT4233),
887 *h$^-$ gpa1.QL ras1Δ* (KT5070) and h$^-$ *MAPKK$^{byr1.DD}$* (KT4194) at times-points 0, 8 ,12 and 24 after
888 mating induction. Note that while the activation induced in the *gpa1.QL* mutant was down-
889 regulated, *MAPKK$^{byr1.DD}$* induced a constitutive activation. Original Western membrane is
890 presented in Fig. S4B. (D) Cell images of the above strains at 12 h after induction of mating. All
891 the cell images were taken and processed as in Figure 1. Scale bar is 10 µm.

892

893 **Fig. 7. Mathematical modelling of the fission yeast pheromone pathway dynamics.**

894 (A) Components and frameworks of the mathematical model in wildtype and signalling mutants:
895 *ras1.G17V*, *Cdc42GEF^{scd1}Δ,* and *MAPKK$^{byr1.DD}$*. Changes corresponding to each mutant are
896 indicated as follows: Grey: removed components or interactions, orange: increased level of
897 activity. For the exact implementation of the mutants, see Materials and Method. The
898 measured component, **pp**MAPK^{Spk1}, is highlighted in green. (B) Measured and simulated
899 **pp**MAPK^{Spk1} activation profiles in wildtype, *ras1.G17V*, *Cdc42GEF^{scd1}Δ* and *MAPKK$^{byr1.DD}$* mutants.
900 Dashed lines: model simulations. Diamonds: experimental data presented in Fig. 1C, E, G, and
901 Fig. 3B; error bars: SEM. (C) GTP-loaded Ras1.G17V (1-172) directly binds to Byr2 (65-180) and
902 Scd1 (760-872). *In vitro* GST pull-down assays of bacterially expressed Ras1.G17V (1-172), GST-
903 Byr2 (65-180) and GST-Scd1 (760-872) were conducted as described in materials and methods.
904 GTP-loaded Ras1.G17V (1-172) was found to bind to both GST-Byr2 (65-180) and GST-Scd1 (760-
905 872). (D) Two Ras1 effectors, Byr2 and Scd1, compete for GTP-loaded Ras1.G17V (1-172). In
906 vitro GST pull-down assays of bacterially expressed Ras1.G17V (1-172) and GST-Byr2 (65-180)
907 were conducted as in (A). Addition of Scd1 (760-872) fragment interfered with Ras1-Byr2

908 binding (the 4th lane). Quantitated signal intensities of the Ras1.G17V (1-172) band in the gel are
909 shown in the right panel. (E) Simulated ppMAPK^{Spk1} dynamics in the wildtype model at
910 increasing concentrations of Ras1^{GTP} added *in silico* to the system. Increased Ras1^{GTP}
911 concentration causes advanced and reduced **pp**MAPK^{Spk1} peak intensities. (F) The model fitted
912 to the 4 strains (as above, in red) correctly predicts ppMAPK^{Spk1} dynamics in the additional 21
913 signalling mutant strains measured in this study.(G) Schematic diagram of the fission yeast
914 pheromone signalling pathway, highlighting the branched pheromone sensing, and that
915 ultimately both branches are necessary for mating.

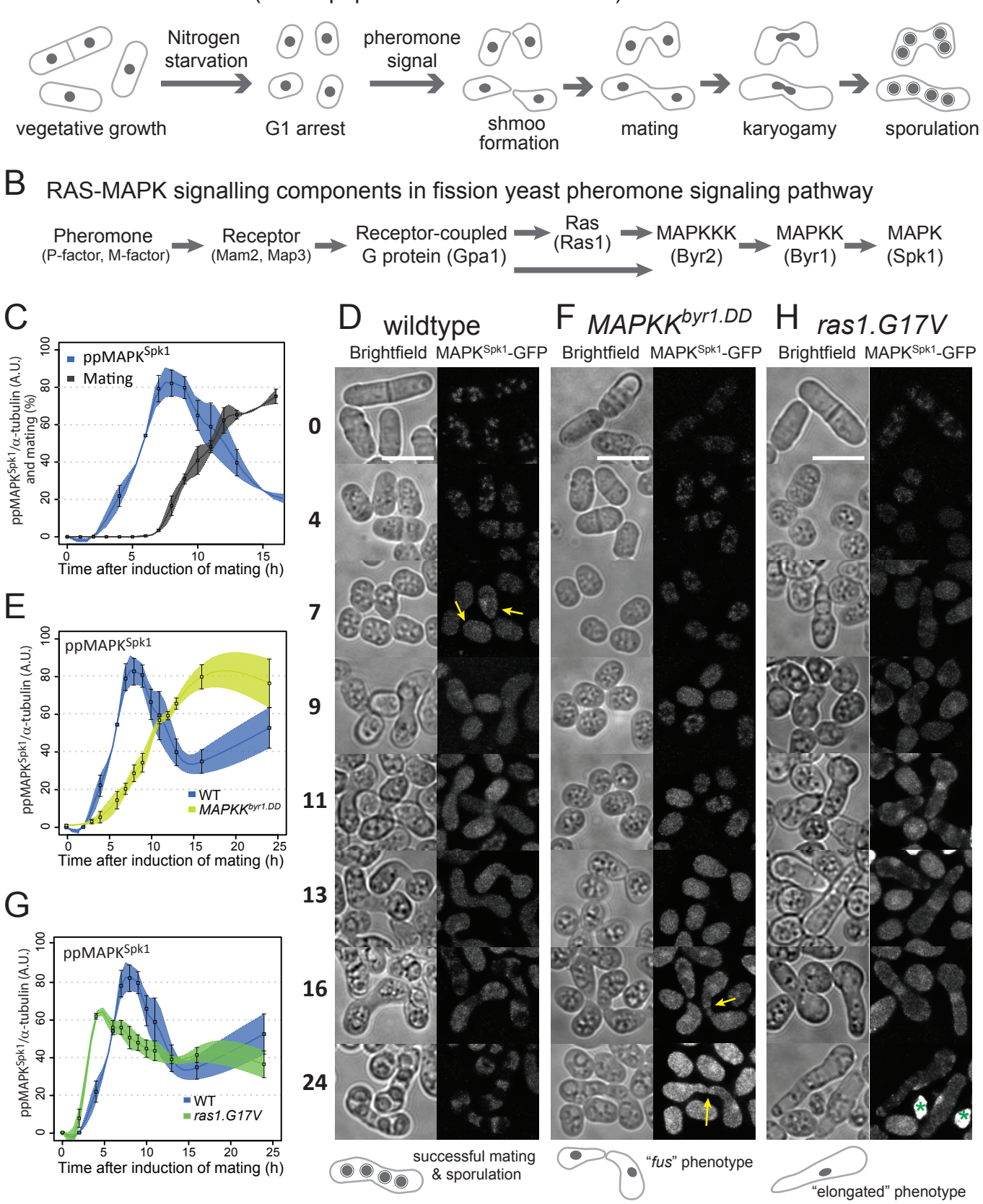

Figure 1. Distinct modes of MAPK^{Spk1} temporal phosphorylation profile and morphological changes during sexual differentiation in wildtype, *MAPKK$^{byr1.DD}$* and *ras1.G17V* mutants.

(A) A pictorial representation of wildtype fission yeast sexual differentiation. (B) A list of key signalling components of the fission yeast pheromone signalling pathway. The diagram reflects the prediction that Gpa1 and Ras1 separately contribute to activation of MAPKKK^{Byr2} activation although the precise mechanism is unknown (Xu et al., 1994). At the same time, Ras1 activation is expected to be at least partly under influence of active Gpa1 because the ste6 gene, encoding a Ras1 activator, is strongly induced upon successful pheromone signaling (Hughes et al., 1994). (C)-(H) Cells were induced for sexual differentiation by the plate mating assay system as described in the materials and methods. (C), (E) and (G) Quantified **pp**MAPK^{Spk1} signal from western blots of wildtype (KT3082) (C), *MAPKK$^{byr1.DD}$* (KT3435) (E) and *ras1.G17V* (KT3084) (G) cells. Three biological replicates were used for quantitation (error bars are ±SEM). α-tubulin was used as a loading control and quantitation was carried out using the Image Studio ver2.1 software (Licor Odyssey CLx Scanner). For the wildtype samples in (C), the % of cells mating is also indicated. The wildtype **pp**MAPK^{Spk1} result (C) is also presented in (E) and (G) as a reference. (D), (F) and (H) Cellular morphology (brightfield) and localization of MAPK^{Spk1}-GFP over a 24 hour time-course in wildtype (D), *MAPKK$^{byr1.DD}$* (F) and *ras1.G17V* (H) cells. Time after induction of mating in hours is indicated on the left. At each time point, a bright-field image and a GFP signal image were taken and processed as described in materials and methods. Green asterisks in the time 24 h in the ras1.G17V cell image (H) indicate auto-fluorescence signal from inviable cell debris, which were presumably produced through cytokinesis failure or cell lysis. Yellow arrows in panels (D) and (F) indicate transient accumulation of MAPK^{Spk1}-GFP at the shmoo tips. Scale bars represent 10μm.

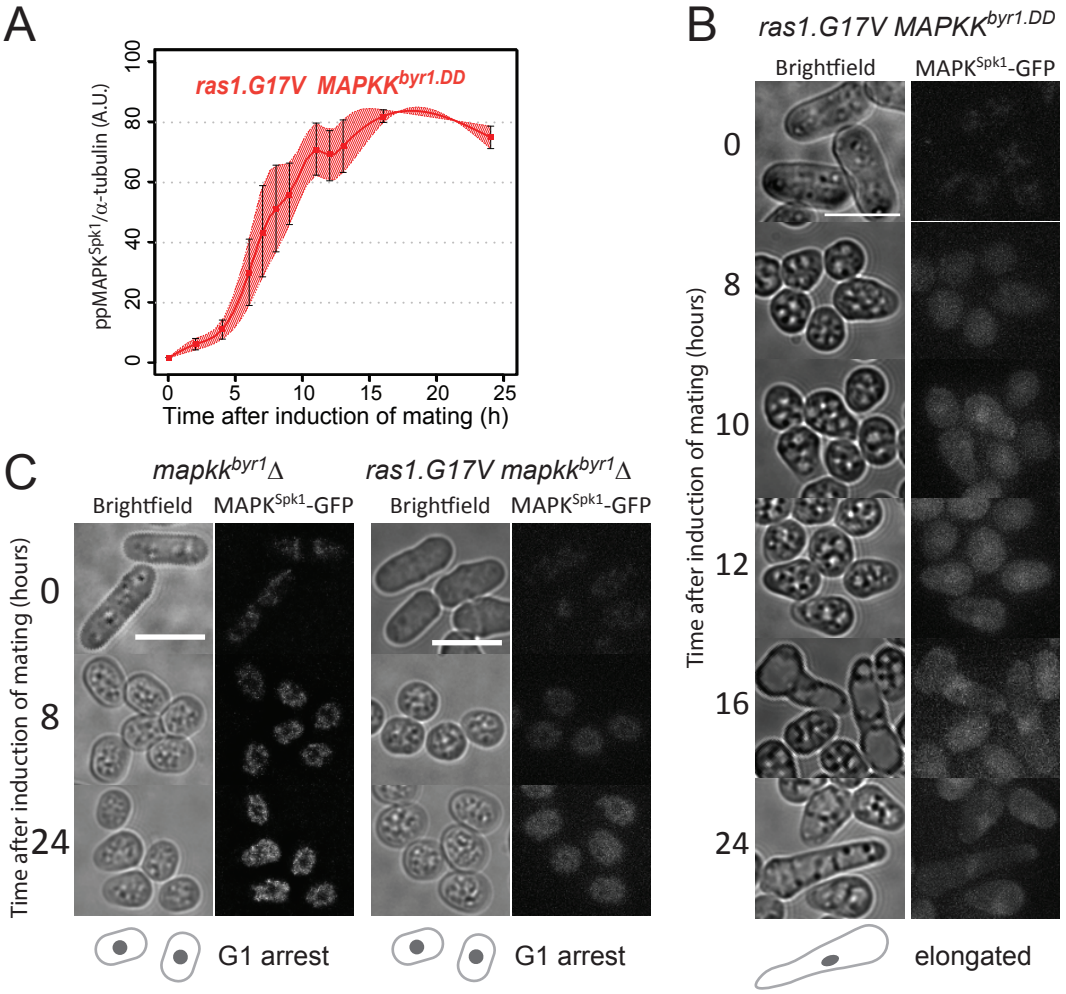

Figure 2. In the *ras1.G17V MAPKK$^{byr1.DD}$* double mutant, the MAPK^{Spk1} phosphorylation profile follows *MAPKK$^{byr1.DD}$* single mutant phenotype whilst cell morphology mimics the *ras1.G17V* single mutant phenotype.

(A) MAPK^{Spk1} phosphorylation status in the *ras1.G17V MAPKK$^{byr1.DD}$* double mutant cells (KT3439). Cells were induced for mating by the plate mating assay system as described in the materials and methods. Quantitated **pp**MAPK^{Spk1} signal (arbitrary unit) from western blots is presented. Results of two biological replicates (each derived from three technical replicates, error bars are ±SEM) are presented in red. (B) The terminal mating phenotype of *ras1.G17V MAPKK$^{byr1.DD}$* double mutant is a phenocopy of *ras1.G17V* single mutant which shows the "elongated" morphology. Images were taken of *ras1.G17V MAPKK$^{byr1.DD}$* double mutant (KT3439) in the same way as in Fig. 1. Time after induction of mating in hours is indicated on the left. (C) There is no morphological change in the absence of MAPK^{Spk1} signalling. Cell images of *MAPKK^{byr1}Δ* (KT4700) and *ras1.G17V MAPKK$^{byr1.DD}$* (KT5030) strains are shown. Images were taken in the same way as in Fig. 1. Time after induction of mating in hours is indicated on the left of each series. Scale bars represent 10μm.

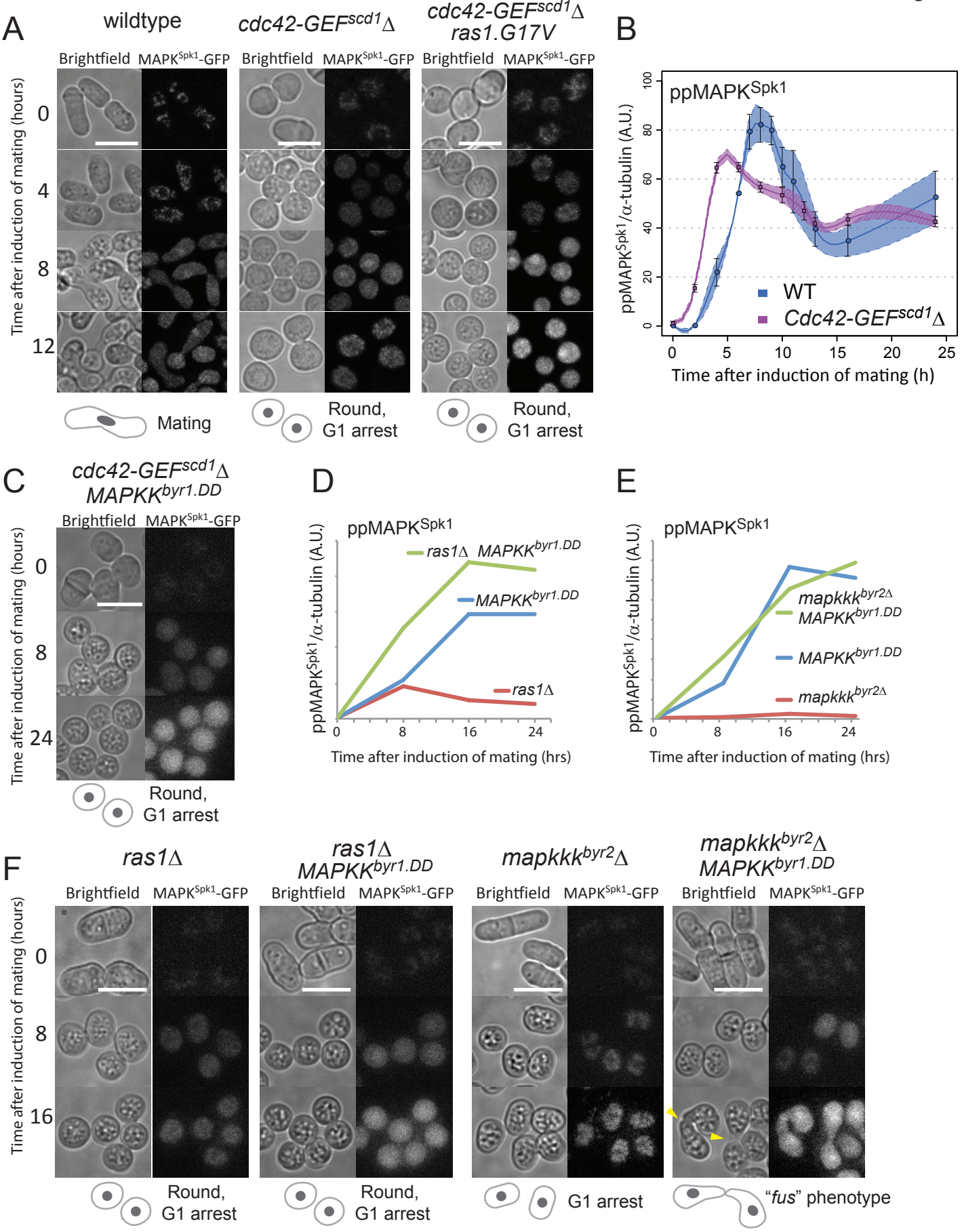

Figure 3. Ras1 activates both MAPK^{Spk1} and Cdc42 pathways during pheromone signalling.
(A) *scd1Δ* morphology and MAPK^{Spk1}-GFP signal. Images of WT (KT3082), *scd1Δ* (KT4061) and *scd1Δ ras1.G17V* double mutant (KT4056) were taken in the same way as in Fig.1. Numbers on the left represents hours after induction of mating. (B) MAPK^{Spk1} phosphorylation state in *scd1Δ* (KT4061) cells after mating induction. Results of three biological replicates (error bars are ±SEM) are presented. The wildtype result presented in Fig.1 (C) is also shown in blue as a reference. (C) Cell images of *scd1Δ MAPKK$^{byr1.DD}$* double mutant (KT4047) were taken in the same way as in Fig.1. Numbers on the left represents hours after induction of mating. (D) MAPK^{Spk1} phosphorylation state in *ras1Δ* (KT4323), *MAPKK$^{byr1.DD}$* (KT3435) and *scd1Δ MAPKK$^{byr1.DD}$* (KT4359) cell extracts. Original Western blotting data is presented in Fig. S3A. (E) MAPK^{Spk1} phosphorylation state in *mapkkk^{byr2}Δ* (KT3763), *MAPKK$^{byr1.DD}$* (KT3435) and *mapkkk^{byr2}Δ MAPKK$^{byr1.DD}$* (KT4010) cell extracts. Original Western blotting data is presented in Fig. S3B. For (D) and (E), quantification was carried out using the Image Studio ver2.1 (Li-cor). (F) Cell images of the strains mentioned in (D) and (E) were taken in the same way as in Fig.1. Numbers on the left represents hours after induction of mating. For all the images presented in (A), (C) and (F), scale bars represent 10μm.

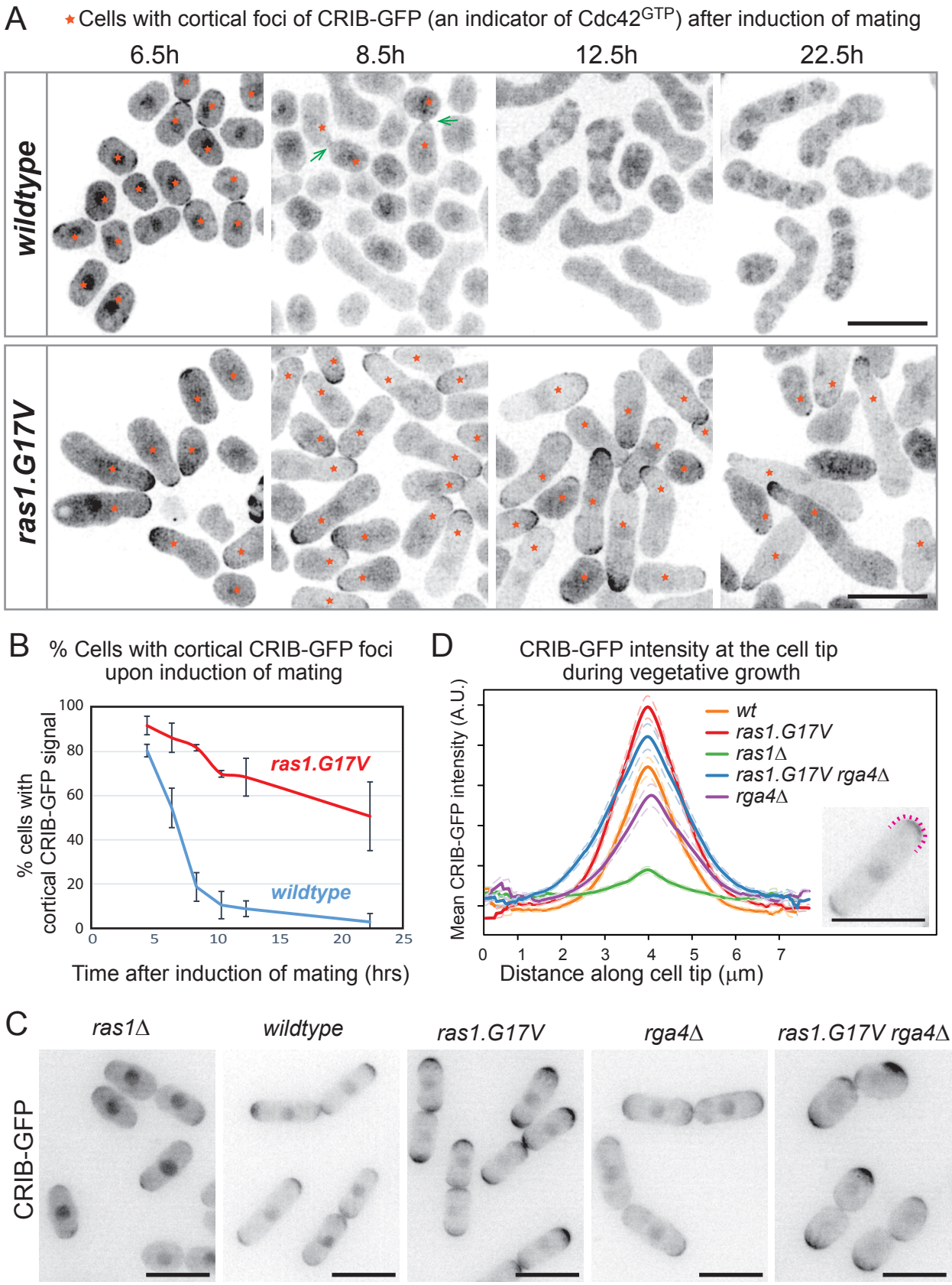

Figure 4. Ras1.G17V induces cortical Cdc42^{GTP} accumulation

(A) Cell morphology and localisation of Cdc42^{GTP}, indicated by CRIB-GFP signal, during the sexual differentiation process. Wildtype (KT5077) and *ras1.G17V* (KT5082) mutant cells were induced for sexual differentiation by the plate mating assay condition (Materials and Methods) and live cell images were taken at the indicated time after induction of mating/sexual differentiation. Representative CRIB-GFP signal images are presented. Cells with cortical CRIB-GFP foci are indicated by orange stars. Rapidly-disappearing CRIB-GFP signals at the fusion site of wildtype mating cells are indicated by green arrows at time 8.5h image. Scale bar: 10 μm. (B) Quantitation of the results presented in (A). At each time point (4.5h, 6.5h, 10.5h, 12.5h and 22.5h after induction of mating/sexual differentiation), 150 cells were examined whether they have cortical CRIB-GFP foci. % cells with cortical CRIB-GFP foci is presented. The experiment was repeated for three times and the mean values and SDs are plotted in the graph. (C) Cell morphology and localisation of Cdc42^{GTP}, indicated by CRIB-GFP signal, during vegetative growth. Representative CRIB-GFP signal images of cells of wildtype (KT5077), *ras1Δ* (5107), *ras1.G17V* (KT5082), *rga4Δ* (5551) and *rga4Δ ras1.G17V* (KT5554) are presented. Scale bar: 10 μm. (D) Quantitated CRIB-GFP signals on the cell cortex of cells presented in (C). Intensity of GFP signal on the cell cortex was measured along one of the cell tips as indicated as a magenta dotted line in the example image on the right (Scale bar: 10 μm) as stated in the Materials and Methods. 40 cells without septum were measured for each strain and the average curve from all aligned traces per strain was calculated, and displayed with respective standard error of the mean curves (dashed lines) as described in Materials and Methods.

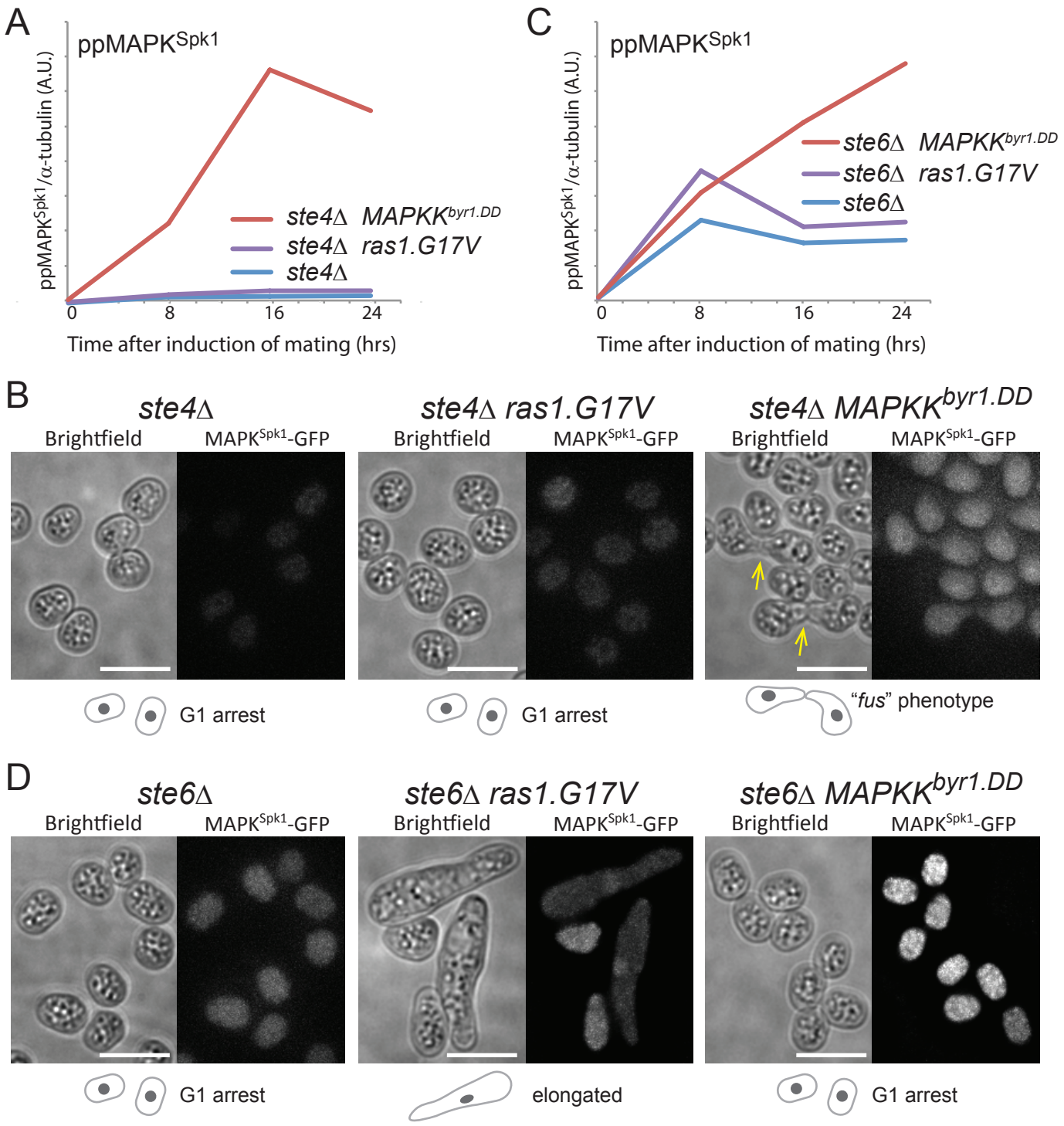

Fig. 5. Distinct contributions of Ste4 and Ste6 to MAPK^{Spk1} phosphorylation.
(A) Ste4 is essential for MAPK^{Spk1} activation. MAPK^{Spk1} phosphorylation status in *ste4Δ* (KT4376), *ste4Δ ras1.G17V* (KT5143) and *ste4Δ MAPKK$^{byr1.DD}$* (KT5136) at times-points 0, 8 ,16 and 24 hours post mating induction are presented. Original Western blotting membranes are presented in Fig. S3C. (B) Incapability of *ste4Δ* to cause pheromone-induced morphological change is suppressed by *MAPKK$^{byr1.DD}$* but not by *ras1.G17V*. Cell images of *ste4Δ* (KT4376), *ste4Δ ras1.G17V* (KT5143) and *ste4Δ MAPKK$^{byr1.DD}$* (KT5136) strains were taken 24 hours after induction of mating. Scale bar: 10 μm. (C) Lack of Ste6 does not result in the complete loss of MAPK^{Spk1} phosphorylation. MAPK^{Spk1} phosphorylation status in *ste6Δ* (KT4333), *ste6Δ ras1.G17V* (KT4998) and *ste6Δ MAPKK$^{byr1.DD}$* (KT5139) at times-points 0, 8 ,16 and 24 hours post mating induction are presented. Original Western blotting membranes are presented in Fig. S3D. (D) Incapability of *ste6Δ* to cause pheromone-induced morphological change is suppressed by *ras1.G17V* mutation but not by *MAPKK$^{byr1.DD}$* mutation. Cell images of *ste6Δ* (KT4333), *ste6Δ ras1.G17V* (KT4998) and *ste6Δ MAPKK$^{byr1.DD}$* (KT5139) strains were taken 24 hours after induction of mating. Scale bar: 10 μm.

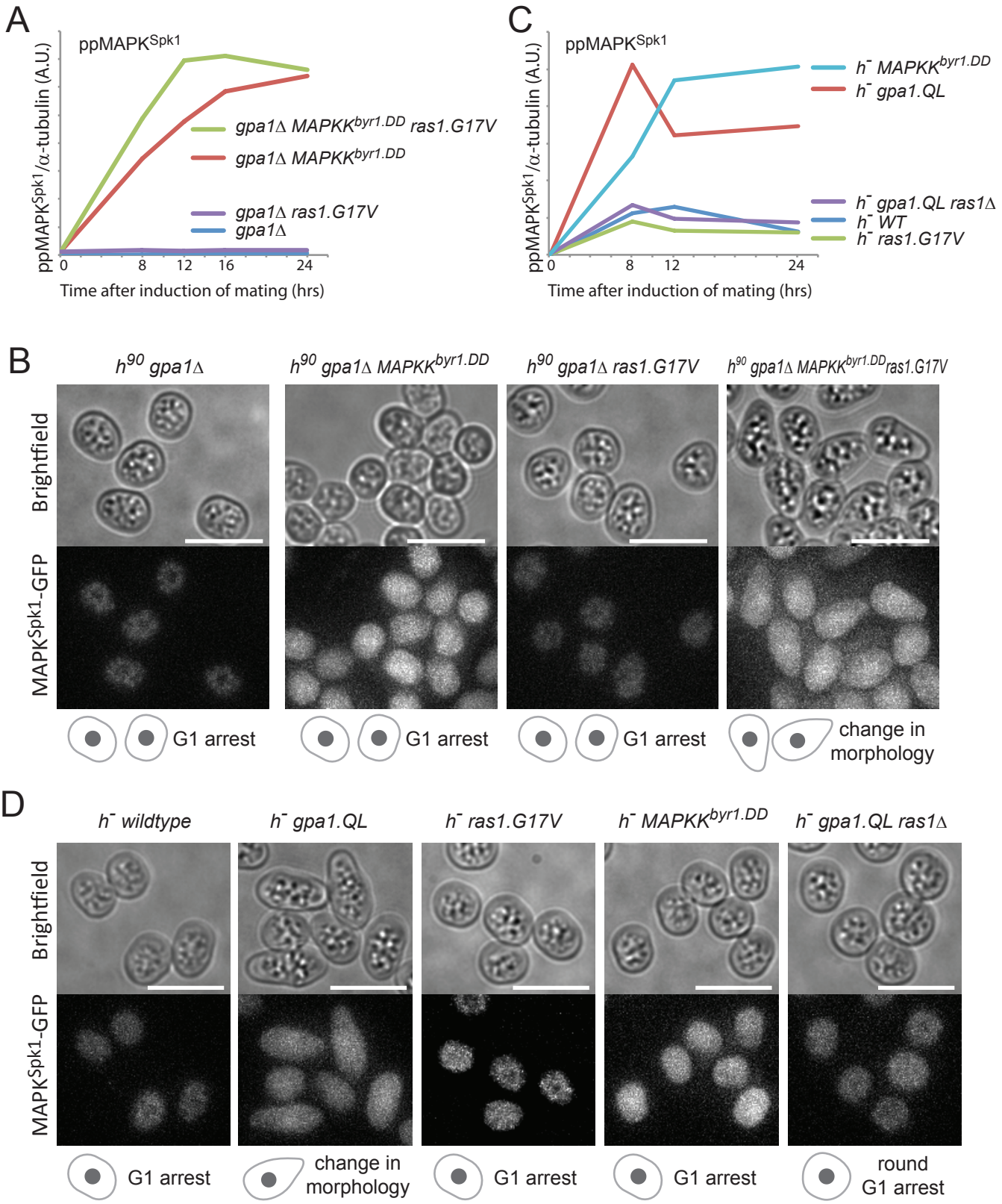

Fig. 6. Gpa1 transduces the pheromone signalling by activating MAPK^{Spk1} and Ras1 pathways.
(A) MAPK^{Spk1} phosphorylation status in homothallic *gpa1Δ* (KT4335), *gpa1Δ ras1.G17V* (KT5023), *gpa1Δ MAPKK$^{byr1.DD}$* (KT4353) and *gpa1Δ ras1.val17 MAPKK$^{byr1.DD}$* (KT5035) at times-points 0, 8 ,12, 16 and 24 hours after mating induction. Original Western membrane is presented in Fig. S4A. (B) Cell images of the above mentioned strains at 16 hours after mating induction. All the cell images were taken and processed as in Figure 1. Scale bar is 10 μm. (C) MAPK^{Spk1} phosphorylation status in *h⁻* WT (KT4190), *h⁻ gpa1.QL* (KT5059), *h⁻ ras1.G17V* (KT4233), *h⁻ gpa1.QL ras1Δ* (KT5070) and *h⁻ MAPKK$^{byr1.DD}$* (KT4194) at times-points 0, 8 ,12 and 24 after mating induction. Note that while the activation induced in the gpa1.QL mutant was down-regulated, *MAPKK$^{byr1.DD}$* induced a constitutive activation. Original Western membrane is presented in Fig. S4B. (D) Cell images of the above strains at 12 h after induction of mating. All the cell images were taken and processed as in Figure 1. Scale bar is 10 μm.

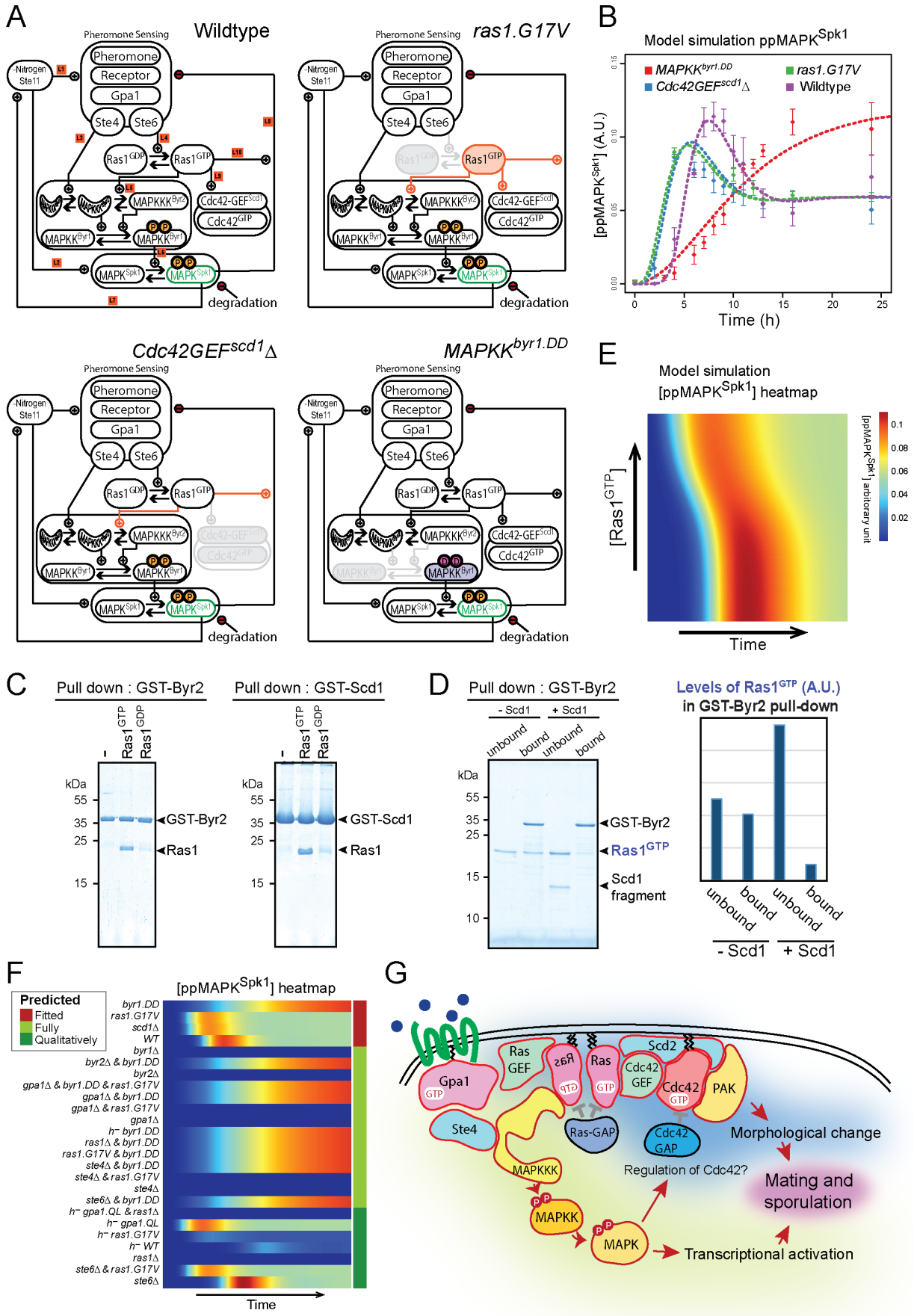

Fig. 7. Mathematical modelling of the fission yeast pheromone pathway dynamics.
(A) Components and frameworks of the mathematical model in wildtype and signalling mutants: *ras1.G17V, Cdc42GEF^{scd1}Δ*, and *MAPKK$^{byr1.DD}$*. Changes corresponding to each mutant are indicated as follows: Grey: removed components or interactions, orange: increased level of activity. For the exact implementation of the mutants, see Materials and Method. The measured component, **pp**MAPK^{Spk1}, is highlighted in green. (B) Measured and simulated **pp**MAPK^{Spk1} activation profiles in wildtype, *ras1.G17V, Cdc42GEF^{scd1}Δ* and *MAPKK$^{byr1.DD}$* mutants. Dashed lines: model simulations. Diamonds: experimental data presented in Fig. 1C, E, G, and Fig. 3B; error bars: SEM. (C) GTP-loaded Ras1.G17V (1-172) directly binds to Byr2 (65-180) and Scd1 (760-872). *In vitro* GST pull-down assays of bacterially expressed Ras1.G17V (1-172), GST-Byr2 (65-180) and GST-Scd1 (760-872) were conducted as described in materials and methods. GTP-loaded Ras1.G17V (1-172) was found to bind to both GST-Byr2 (65-180) and GST-Scd1 (760-872). (D) Two Ras1 effectors, Byr2 and Scd1, compete for GTP-loaded Ras1.G17V (1-172). *In vitro* GST pull-down assays of bacterially expressed Ras1.G17V (1-172) and GST-Byr2 (65-180) were conducted as in (A). Addition of Scd1 (760-872) fragment interfered with Ras1-Byr2 binding (the 4th lane). Quantitated signal

intensities of the Ras1.G17V (1-172) band in the gel are shown in the right panel. (E) Simulated ppMAPK^{Spk1} dynamics in the wildtype model at increasing concentrations of Ras1^{GTP} added *in silico* to the system. Increased Ras1^{GTP} concentration causes advanced and reduced **pp**MAPK^{Spk1} peak intensities. (F) The model fitted to the 4 strains (as above, in red) correctly predicts ppMAPK^{Spk1} dynamics in the additional 21 signalling mutant strains measured in this study.(G) Schematic diagram of the fission yeast pheromone signalling pathway, highlighting the branched pheromone sensing, and that ultimately both branches are necessary for mating.